Journal of the Iranian Chemical Society (2022) 19:521–545
https://doi.org/10.1007/s13738-021-02319-4

ORIGINAL PAPER

Synthesis, molecular docking, and in silico ADME prediction of some fused pyrazolo[1,5-*a*]pyrimidine and pyrazole derivatives as potential antimicrobial agents

Ashraf S. Hassan[1] · Nesrin M. Morsy[1] · Hassan M. Awad[2] · Ahmed Ragab[3]

Received: 29 March 2021 / Accepted: 20 June 2021 / Published online: 26 June 2021

Abstract

Twenty compounds of pyrazolo[1,5-*a*]pyrimidines **14a–j** and pyrazole derivatives as Schiff bases **16a–j** have been synthesized by the reaction of 5-amino-pyrazole derivatives **9a**, **b** with 2-(arylidene)malononitriles **10a–e** or various aldehydes **15a–e**, respectively. The biological activity of the pyrazolo[1,5-*a*]pyrimidines **14a–j** and pyrazole derivatives **16a–j** was evaluated and showed a variation in antimicrobial inhibitory activity. In particular, the three pyrazolo[1,5-*a*]pyrimidines (**14b**, **14e,** and **14j**) and four pyrazole Schiff bases (**16c**, **16d**, **16 h,** and **16i**) have possessed a broad spectrum of activity with the inhibition zone range from 15 to 20 mm. Also, the structure–activity relationship study was done. Furthermore, physicochemical properties, drug-likeness model score, bioactivity scores, ADME, and toxicity properties were predicted in silico and some products possessed acceptable and a good results. Finally, the molecular docking studies performed inside the active site of DNA gyrase (PDB: 2XCT), the secreted aspartic protease from *C. albicans* (PDB: 1ZAP), and exhibited lower binding energy with different types of binding mode. Besides, the electrostatic potential maps were generated to determine the charge distribution around a molecule and therefore determine the regions that could form hydrogen bonding donors and acceptors that confirmed the binding mode in the docking study. The results suggested that these derivatives could act as antimicrobial agents.

✉ Ashraf S. Hassan
ashraf_salmoon@yahoo.com

✉ Ahmed Ragab
Ahmed_ragab@azhar.edu.eg

[1] Organometallic and Organometalloid Chemistry Department, National Research Centre, Dokki, Cairo 12622, Egypt

[2] Chemistry of Natural and Microbial Products Department, Pharmaceutical and Drug Industries Research Division, National Research Centre, Dokki, Cairo 12622, Egypt

[3] Department of Chemistry, Faculty of Science (Boys), Al-Azhar University, Nasr City, Cairo 11884, Egypt

Graphic abstract

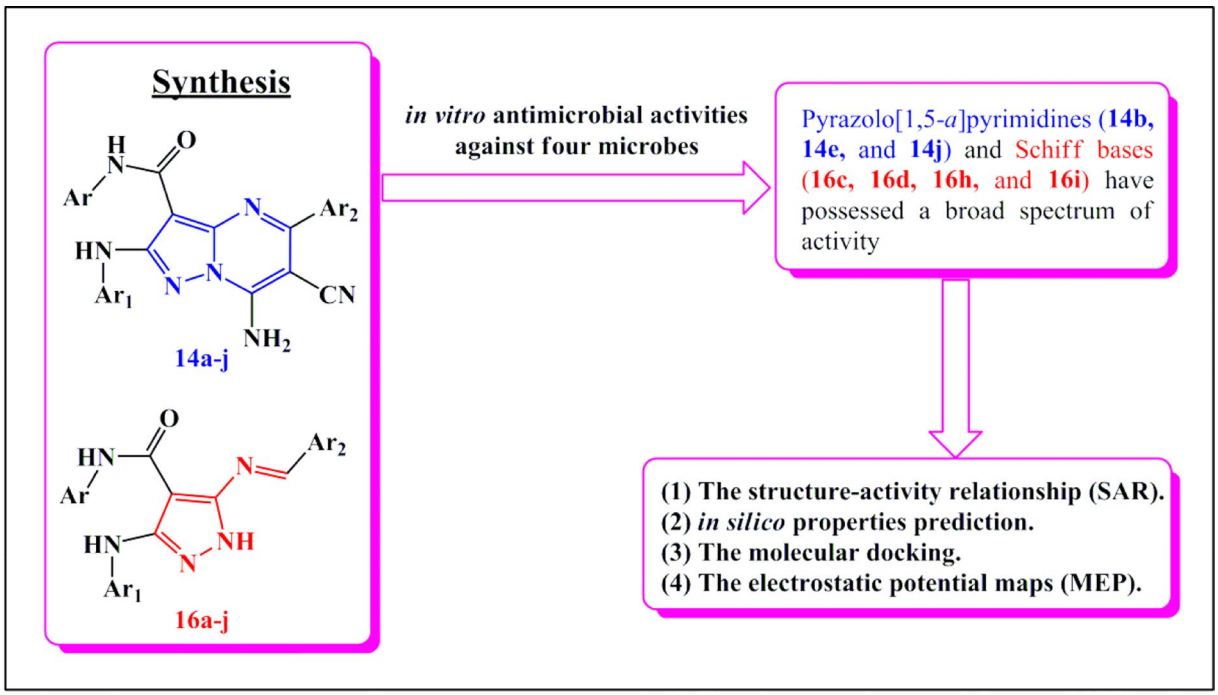

Introduction

The important tasks of the researchers in the medical, pharmaceutical, and chemical fields are the design and preparation of bioactive compounds to overcome some health problems such as cancer and bacterial infectious diseases. Therefore, there is a growing interest in the preparation of pyrazolo[1,5-*a*]pyrimidines derivatives due to their biological applications as promising antimicrobial, anticancer, antitubercular, and enzyme inhibitors [1–6]. For example, pyrazolo[1,5-*a*]pyrimidine-3-carbonitrile derivative **1** was synthesized by Attia et al., as a promising anti-proliferative agent against the MCF-7 cell line [7]. The two water-soluble pyrazolo[1,5-*a*]pyrimidine derivatives (**2** and **3**) were synthesized and characterized with antibacterial activity against *Escherichia coli* [8]. Also, from our previous studies, the two pyrazolo[1,5-*a*]pyrimidine derivatives {5,7-dimethylpyrazolo[1,5-*a*]pyrimidine derivative **4** and 7-phenylpyrazolo[1,5-*a*]pyrimidine derivative **5**} were prepared and displayed a promising antimicrobial agent [9] and antitumor agent against HepG-2 cells [10], respectively (Fig. 1). Moreover, the pyrazolopyrimidine structure is present in drugs such as Dinaciclib, Anagliptin, and Ocinaplon [11].

Besides, pyrazole Schiff bases (pyrazole-azomethine) are known to have a vast spectrum of biological activities such as antimicrobial, antitumor, immunomodulatory, analgesic, DNA binding, and DHFR/DNA gyrase inhibitors [12–18]. In 2013, Malladi and co-workers have described a synthesis of compound triazole-pyrazole Schiff base **6** which exhibited promising antibacterial activity against *Staphylococcus aureus* [19]. Recently, in 2020, Hassan et al., prepared two furan-pyrazole Schiff bases **7** and **8** as *Nitrofurantoin*® analogues which exhibited antibacterial activities against *Escherichia coli* and *Salmonella typhimurium* bacteria [20] (Fig. 1).

Because of the biological importance of pyrazolo[1,5-*a*]pyrimidines, pyrazole Schiff bases, and in continuation of our program for synthesis bioactive compounds [21–40]. In this work, we have synthesized 5-amino-*N*-aryl-1*H*-pyrazole-4-carboxamides **9a**, **b** [41] as starting materials for the preparation of new 5-aryl-7-amino-pyrazolo[1,5-*a*]pyrimidines **14a–j** and pyrazole Schiff bases **16a–j** for evaluation of their antimicrobial properties as well as the structure–activity relationship (SAR), the molecular docking, the electrostatic potential maps (MEP), and in silico properties prediction were studied (Fig. 2).

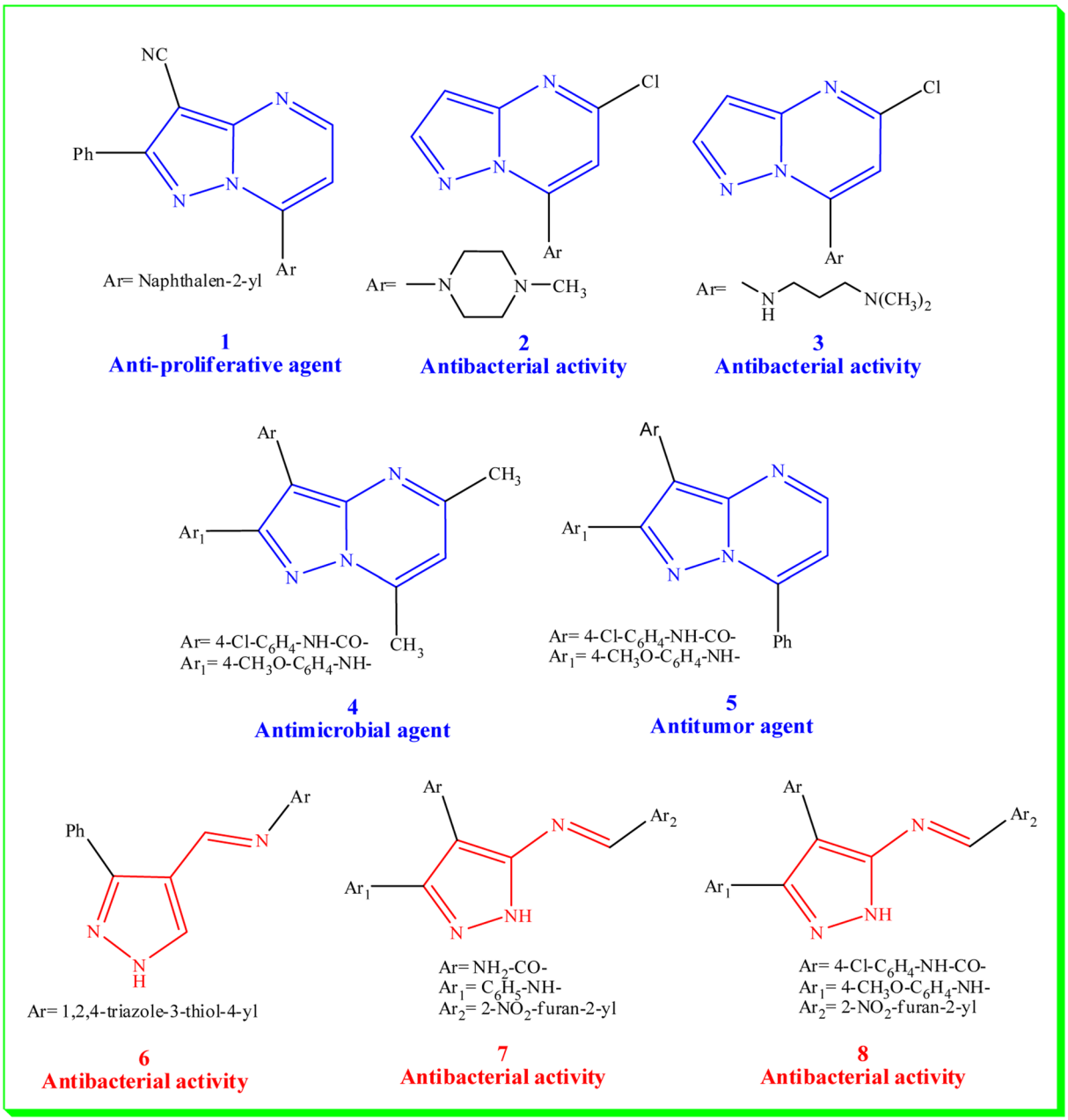

Fig. 1 Biological applications of pyrazolopyrimidines **1–5** and pyrazole Schiff bases **6–8**

Result and discussion

Chemistry

The target compounds, pyrazolo[1,5-*a*]pyrimidines **14a–j** and pyrazole Schiff bases **16a–j**, are shown in Schemes 1 and 2. The starting materials, 5-amino-pyrazole derivatives **9a**, **b** and 2-(arylidene)malononitriles **10a–e,** were prepared according to previously reported methods [42, 43] and are described in Scheme 3.

A series of 7-amino-pyrazolo[1,5-*a*]pyrimidines **14a–j** were prepared via the reaction of 5-amino-*N*-aryl-1*H*-pyrazole-4-carboxamides **9a**, **b** with 2-(arylidene)malononitriles **10a–e** in refluxing ethanol (Scheme 1). This reaction involves nucleophilic addition of amino group of **9a, b** to double bond of 2-(arylidene)malononitriles **10a–e** to produce the intermediate 5-((2,2-dicyano-1-phenylethyl) amino)-1*H*-pyrazole derivative **11a–j**. Furthermore, the cyclic imino group in intermediate 1*H*-pyrazole derivative **11a–j** acts as nucleophile to cyano group to obtain 7-imino-pyrazolo[1,5-*a*]pyrimidine-3-carboxamide

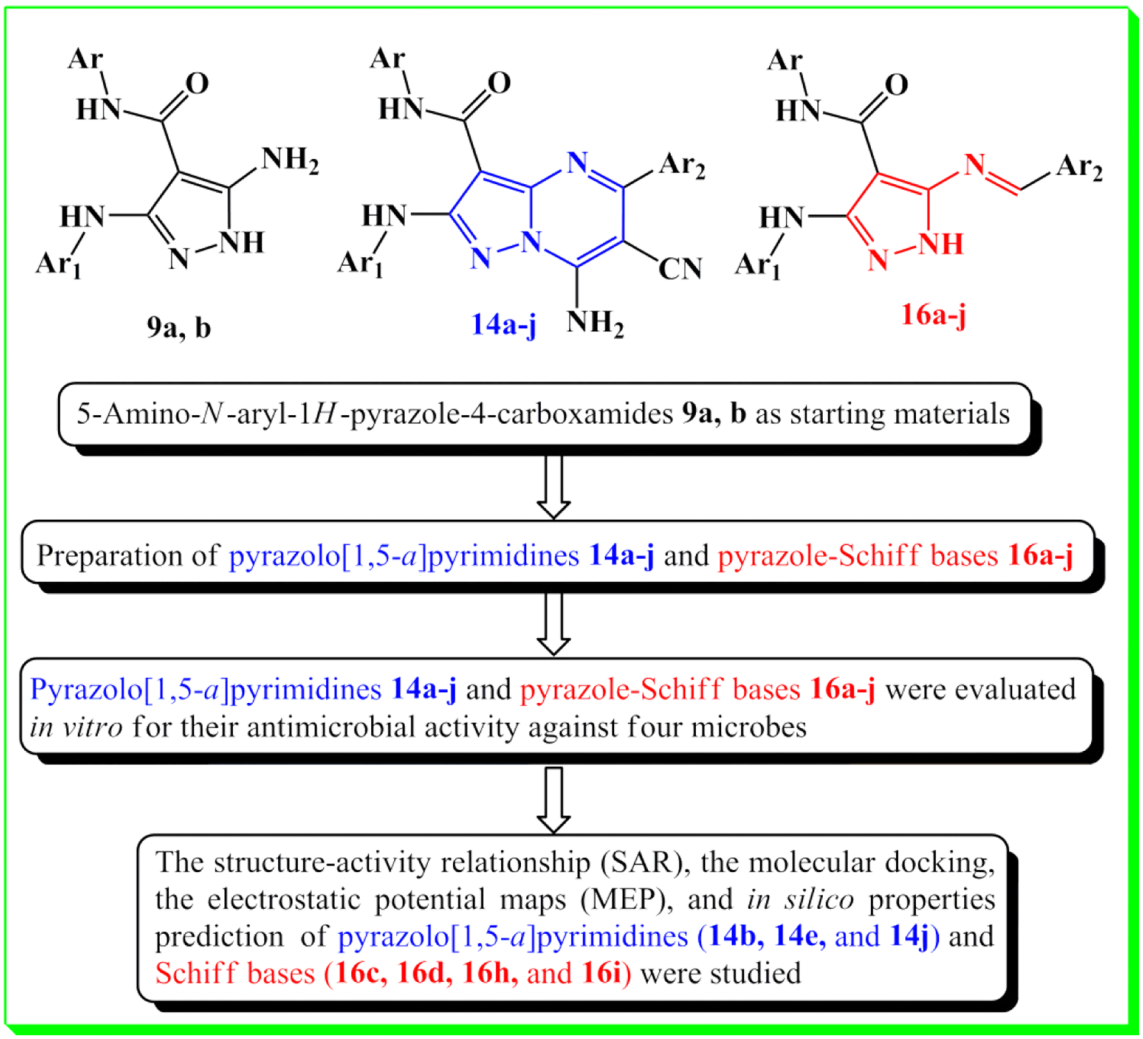

Fig. 2 The target compounds (**14a–j** and **16a–j**) and their studies

derivatives **12a–j** that underwent proton shift and oxidation to afford the corresponding 7-amino-pyrazolo[1,5-*a*] pyrimidine derivatives **14a–j**.

The structure of 7-amino-pyrazolo[1,5-*a*]pyrimidines structures **14a–j** was confirmed by spectral data and elemental analysis. The IR spectrum of 7-amino-pyrazolo[1,5-*a*]pyrimidine derivative **14a** was characterized by appearing new band for C≡N group at ν 2213 cm^{-1} and two bands at ν 3428 and 3304 cm^{-1} for NH_2 and 2NH groups. Also, the C=O amide group appeared at ν 1641 cm^{-1}. The mass spectrum of pyrazolo[1,5-*a*]pyrimidine derivative **14a** was exhibited a molecular ion pack at *m/z* 489 with intensity 17.65% corresponding to the formula $C_{28}H_{23}N_7O_2$ (489.53) and the base peak at *m/z* 396 (100%). The ^{1}H NMR (δ/ppm) spectrum of **14a** exhibited two signals at δ 2.43 and 3.74 ppm assigned to the protons of CH_3 and OCH_3 groups, respectively. Besides, the NH_2 group appeared as a broad signal at δ 9.00 ppm, and two exchangeable singlet signals at δ 9.23 and 10.14 ppm corresponding to two NH groups.

The three aromatic rings (Figure S1, Supplementary Material) were interpreted as the following:

(i) Phenyl ring (five protons) appeared as two triplets at δ 7.09 ppm (1H, J = 7.5 Hz) and δ 7.37 ppm (2H, J = 7.8 Hz) and one doublet at δ 7.60 ppm (2H, J = 7.7 Hz).
(ii) 4-Methoxyphenyl ring (4 protons, AB-system) appeared as two doublets at δ 6.90 (2H) and 7.84 (2H) ppm (each with J (coupling constant) = 9.0 Hz).
(iii) 4-Methylphenyl ring (4 protons, *AB-system*) appeared as two doublets at δ 7.44 (2H) and 7.90 (2H) ppm (each with J (coupling constant) = 8.2 Hz).

Additionally, the ^{13}C NMR spectrum of **14a** exhibited characterized signals of CH_3 and –OCH_3 carbon at δ 21.19

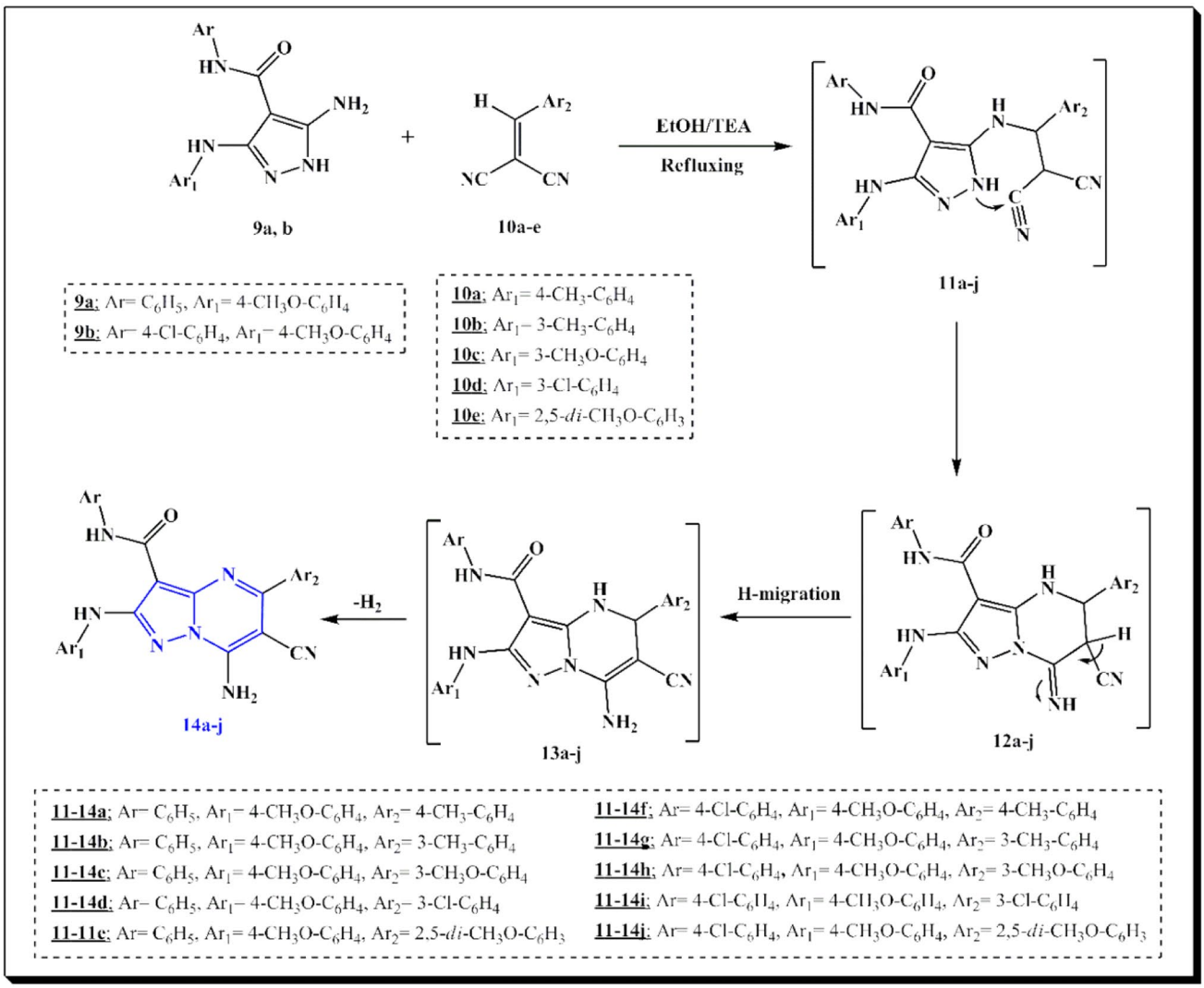

Scheme 1 Synthesis of pyrazolo[1,5-*a*]pyrimidines **14a–j**

and 55.26 ppm, respectively. The rest of carbon atoms (26 carbon) of 7-amino-pyrazolo[1,5-*a*]pyrimidine derivative **14a** have appeared ranged between δ 74.88–145.70 ppm as well as signals at δ 149.49, 153.98, 156.32, 161.47, and 162.29 ppm corresponding to two C=N, carbonyl group, carbon attached to methoxy (C–OMe), and carbon attached to an amino group (C-NH_2), respectively.

Moreover, the 5-(2,5-dimethoxyphenyl)-pyrazolo[1,5-*a*] pyrimidine-3-carboxamide derivative **14j** was another example of the ^{1}H NMR spectra, exhibited three singlet signals at δ 3.70, 3.75, and 3.78 ppm for the three methoxy groups. The aromatics protons appeared at δ 6.86 (d, 2H, J = 9.5 Hz, *p*-methoxyphenyl ring), 7.10–7.17 (m, 3H, 2, 5-dimethoxyphenyl ring), 7.34 (d, 2H, J = 9.2 Hz, *p*-chlorophenyl ring), 7.48 (d, 2H, J = 9.2 Hz, *p*-chlorophenyl ring), and 7.78 (d, 2H, J = 9.3 Hz, *p*-methoxyphenyl ring). Further, three exchangeable singlet signals appeared as the broad peak at δ 8.97 ppm, and two signals at δ 9.11 and 10.04 ppm refer to the protons of the amino group (NH_2) as well as two NH groups, respectively. The ^{13}C NMR spectrum of **14j** exhibited characterized signals of three methoxy carbons at δ 55.12, 55.68, and 55.93 ppm. The rest of carbon atoms (26 carbon) of **14j** have appeared at δ 78.02, 88.84, 104.95, 113.21, 114.13, 115.17, 117.23, 118.96, 120.38, 126.91, 128.90, 133.25, 137.20, 145.72, 148.51, 150.65, 153.07, 153.91, 156.07, 159.97, 159.99, and 162.09 ppm. Also, the structure of 7-amino-pyrazolo[1,5-*a*]pyrimidine derivatives **14a–j** and reaction mechanism pathway was proved from our previous study through X-ray single-crystal analysis of analogues [44].

Schiff bases **16a–j** were prepared via the reaction of 5-amino-pyrazoles **9a**, **b** with various aldehydes **15a–e** in refluxing absolute ethanol (Scheme 2). Schiff bases structure **16a–j** was confirmed by spectral analysis. The IR spectrum

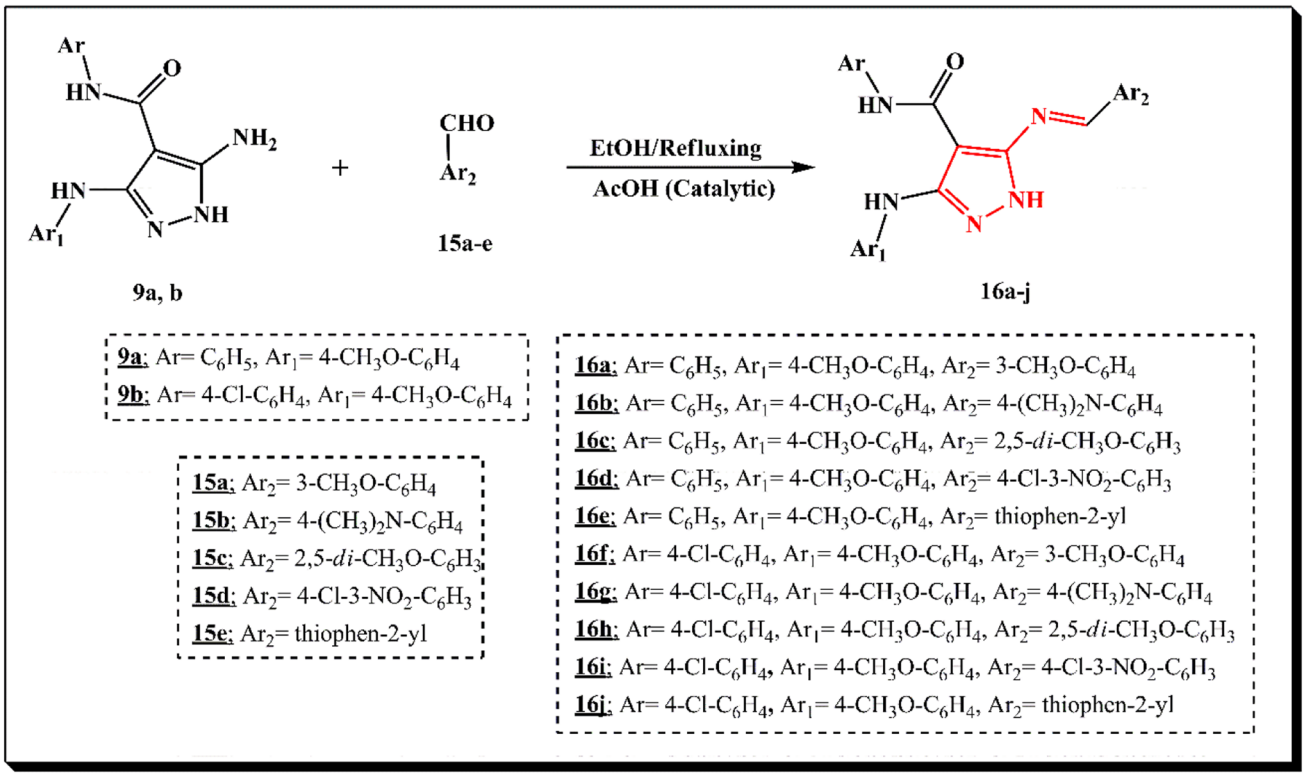

Scheme 2 Synthesis of Schiff bases **16a–j**

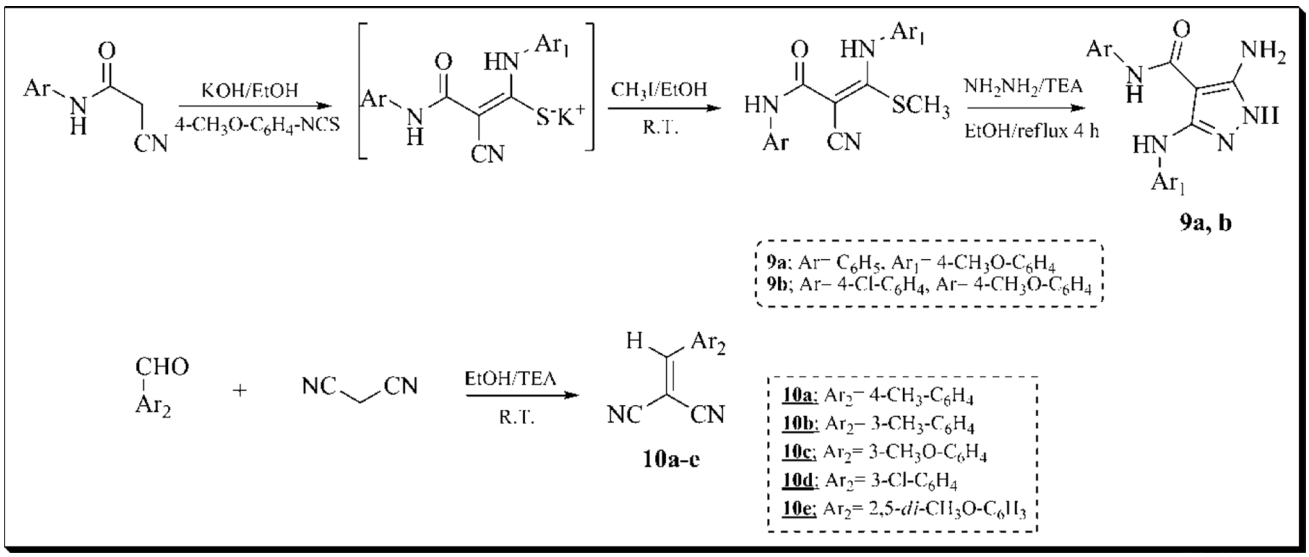

Scheme 3 Synthesis of starting materials (**9a, b** and **10a–e**)

of azomethine derivative **16d** displayed bands at ν 3431, 3235, 1635, and 1615 cm^{-1} characteristic for 3NH, carbonyl (C=O), and imino (C=N) groups, respectively. The ^{1}H NMR (δ/ppm) spectrum of 5-(4-chloro-3-nitrobenzylideneamino)-1*H*-pyrazole-4-carboxamide derivative **16d** exhibited one signal at δ 3.70 ppm for the methoxy group. The aromatic protons have appeared at δ 6.89 (d, 2H, J = 8.3 Hz, *p*-methoxyphenyl ring), 7.06 (t, 1H, J = 7.3 Hz, phenyl ring), 7.31–7.34 (m, 4H, phenyl ring), 7.67 (d, 2H, J = 7.9 Hz, *p*-methoxyphenyl ring), 8.00 (d, 1H, J = 8.3, 4-chloro-3-nitrophenyl ring), 8.30 (d, 1H, J = 8.3, 4-chloro-3-nitrophenyl ring), and 8.67 (s, 1H, 4-chloro-3-nitrophenyl ring). The

methine proton (–CH=N–) has appeared at δ 8.76 ppm. Besides, the three exchangeable signals appeared at δ 9.13, 9.79, and 12.80 ppm related to three NH protons.

Additionally, the IR spectrum of pyrazole Schiff base derivative **16f** was characterized by bands for 3NH, C=O, C=N, and C=C groups at ν 3434, 3229, 1656, 1612, and 1587 cm^{-1}, respectively. The ^{1}H NMR (δ/ppm) spectrum of pyrazole derivative **16f** exhibited two signals at δ 3.73 and 3.87 ppm for the protons of two methoxy groups. Besides, the proton of –CH=N– function appeared at δ 8.66 ppm and the protons of the three NH appeared as single signals at δ 9.03, 10.02, and 12.78 ppm. The spectrum has exhibited the protons of the three aromatic rings (Figure S2, Supplementary Material) as.

(i) Two doublets appeared at δ 6.90 (2H, J = 8.9 Hz) and 7.69 (2H, J = 8.9 Hz) for the *p*-methoxyphenyl ring.
(ii) One doublet at δ 7.40 (4H) for the *p*-chlorophenyl ring with J = 8.9 Hz.
(iii) *m*-Methoxyphenyl ring; one proton as a doublet–doublet (dd) at δ 7.23 (J = 8.2 & 1.8 Hz), one proton as a triplet at δ 7.53 (J = 7.9 Hz), single signal at δ 7.59 for one proton, and one doublet for one proton at δ 7.62 (J = 2.4 Hz).

The ^{13}C NMR spectrum of **16f** exhibited characterized signals of two methoxy carbons at δ 55.19 and 55.23 ppm. The rest of 23 carbon atoms appeared at δ 92.61, 112.24, 114.39, 119.22, 119.53, 120.41, 122.48, 126.69, 128.34, 128.73, 130.28, 133.79, 136.17, 137.46, 151.21, 154.04, 159.74, 162.03, and 162.65 ppm.

Antimicrobial evaluation

Pyrazolo[1,5-*a*]pyrimidines **14a–j** and pyrazole Schiff bases **16a–j** were evaluated in vitro for their antimicrobial activity against four microbes using the agar diffusion method [45, 46], and the results are listed in Table 1 and represented in Fig. 3**.**

From the results obtained in Table 1 and Fig. 3, it was found that most of the pyrazolo[1,5-*a*]pyrimidines **14a–j** and pyrazole Schiff bases **16a–j** have a reasonable antimicrobial undertaking impact against most of the tested pathogens in this study. Besides, most of the pyrazolopyrimidines **14a–j** and pyrazole Schiff bases **16a–j** confirmed a diverse inhibitory effect against all pathogenic microorganisms used.

In the case of Bacillus subtilis (G+) bacteria: the three pyrazolopyrimidines [**14b**, **14e** (inhibition zone (IZ) = 20 mm), and **14j** (IZ = 21 mm)] and the pyrazole Schiff base **16i** (IZ = 19 mm) confirmed a strong inhibition effect more than the antibacterial standard used (Tetracycline, IZ = 18 mm). Furthermore, pyrazolopyrimidine **14d** and the pyrazole Schiff bases **16a** (IZ = 18 mm) showed comparable antibacterial activity of the Tetracycline drug (IZ = 18 mm). Both the pyrazolopyrimidine derivatives (**14c** and **14g–i**) and pyrazole Schiff bases (**16c–h** and **16j**) showed a good inhibition with range = 15–17 mm.

In the case of Escherichia coli (G−) bacteria: all the pyrazolo[1,5-*a*] pyrimidines **14a–j** and pyrazole Schiff bases **16a–j** (IZ = 13 to 16 mm) presented from good to an excellent inhibition compared to the Novobiocin (IZ = 16 mm).

Aspergillus niger (Filamentous fungi): Pyrazolopyrimidine **14f** and four pyrazole Schiff bases **(16c, 16d, 16h,** and **16i**) revealed IZ from (18 mm) to (20 mm) and confirmed a robust inhibition impact, while, four pyrazolopyrimidines (**14d, 14e, 14g,** and **14i**) and three Schiff bases (**16a, 16e**, and **16j**) with IZ = 15 mm showed a reasonable inhibitory activity compared to Clotrimazole (IZ = 23 mm) as a positive control. It is worth mentioning that *Aspergillus niger* is one of the fungal pathogens that can affect the respiratory tract. *A. niger* is a causative agent of pulmonary diseases inclusive of aspergillosis, bronchial asthma, and acute allergic alveolitis. The fungus colonizes ancient tuberculosis or bronchi static cavities, in which its varieties a large colony (aspergilloma); or it can also without a doubt invade the lung tissue to produce hemorrhagic and necrotizing pneumonia [47].

In the case of Candida albicans (Yeast): the pyrazolopyrimidines (**14b**, **14d,** and **14f**) and Schiff base **16i** (IZ rang = 17–20 mm) showed a good inhibition effect. Moreover, the pyrazolopyrimidines (**14c, 14e, 14g,** and **14i**) and Schiff bases (**16b, 16c, 16d, 16e, 16g,** and **16h**) showed a moderate inhibition with inhibition zone (IZ) = 15 mm. Further, the pyrazolopyrimidine **14a** (IZ = 13 mm) and two Schiff bases **16a** (IZ = 13 mm) and **16j** (IZ = 12 mm) showed a weak effect in contrast to the antibacterial standard antibiotic Cyclohexamide (IZ = 32 mm).

From the above, the three pyrazolo[1,5-*a*]pyrimidines (**14b**, **14e**, and **14j**) and four pyrazole Schiff bases (**16c**, **16d**, **16h,** and **16i**) proved to be potent against the four microbes tested, possessed a broad spectrum of activity, and in several cases, their activities exceeded the reference drugs used.

Structure activity relationship study

Depending on the structure represented on Schemes 1, 3, and Fig. 4, our synthesis strategy depends on the preparation of two 2-cyano-*N*-(aryl)acetamide, and the aryl represented as phenyl or 4-chlorophenyl. The cyanoacetanilide derivatives reacted with 4-methoxyphenyl isothiocyante and finally refluxed with hydrazine hydrate to produce 5-amino-pyrazole derivatives **9a, b** with two variable aryl groups. The 5-amino-pyrazole derivatives **9a, b** obtained used as key starting materials to form pyrazolo[1,5-*a*]pyrimidine derivatives **14a–j** and azomethine pyrazole derivatives **16a–j**. Generally, most of the target compounds **14a–j** and

Table 1 Antimicrobial activities represented by the mean of Inhibition Zone (IZ) in (mm) of pyrazolo[1,5-*a*]pyrimidines **14a–j,** pyrazole Schiff bases **16a–j,** and standard antibiotics using the agar diffusion method

Compounds	Ar	Ar_1	Ar_2	Bacteria		Fungi	
				(G^+) *B. subtilis* ATCC-6633	(G^-) *E. coli* ATCC-25922	Filamentous *A. niger* NRRL-3	Unicellular *C. albicans* ATCC-10231
14a	Ph	4-$CH_3OC_6H_4$	4-$CH_3C_6H_4$	12	14	0	13
14b	Ph	4-$CH_3OC_6H_4$	3-$CH_3C_6H_4$	20	16	0	17
14c	Ph	4-$CH_3OC_6H_4$	3-$CH_3OC_6H_4$	15	14	0	15
14d	Ph	4-$CH_3OC_6H_4$	3-ClC_6H_4	18	15	15	17
14e	Ph	4-$CH_3OC_6H_4$	2,5-*di*-$CH_3OC_6H_3$	20	16	15	15
14f	4-ClC_6H_4	4-$CH_3OC_6H_4$	4-$CH_3C_6H_4$	13	14	18	18
14g	4-ClC_6H_4	4-$CH_3OC_6H_4$	3-$CH_3C_6H_4$	16	15	15	15
14h	4-ClC_6H_4	4-$CH_3OC_6H_4$	3-$CH_3OC_6H_4$	15	15	0	0
14i	4-ClC_6H_4	4-$CH_3OC_6H_4$	3-ClC_6H_4	16	15	15	15
14j	4-ClC_6H_4	4-$CH_3OC_6H_4$	2,5-*di*-$CH_3OC_6H_3$	21	16	0	0
16a	Ph	4-$CH_3OC_6H_4$	3-$CH_3OC_6H_4$	18	15	15	13
16b	Ph	4-$CH_3OC_6H_4$	4-$(CH_3)_2$ N C_6H_4	12	13	0	15
16c	Ph	4-$CH_3OC_6H_4$	2,5-*di*-$CH_3OC_6H_3$	15	14	20	15
16d	Ph	4-$CH_3OC_6H_4$	4-Cl-3-NO_2-C_6H_3	17	16	20	15
16e	Ph	4-$CH_3OC_6H_4$	Thiophen-2-yl	15	15	15	15
16f	4-ClC_6H_4	4-$CH_3OC_6H_4$	3-$CH_3OC_6H_4$	15	15	0	0
16g	4-ClC_6H_4	4-$CH_3OC_6H_4$	4-$(CH_3)_2$ N C_6H_4	15	14	0	15
16h	4-ClC_6H_4	4-$CH_3OC_6H_4$	2,5-*di*-$CH_3OC_6H_3$	16	15	20	15
16i	4-ClC_6H_4	4-$CH_3OC_6H_4$	4-Cl-3-NO_2-C_6H_3	19	15	20	20
16j	4-ClC_6H_4	4-$CH_3OC_6H_4$	Thiophen-2-yl	16	14	15	12
A	–	–	–	18	–	–	–
B	–	–	–	–	16	–	–
C	–	–	–	–	–	23	–
D	–	–	–	–	–	–	32

Antibacterial Standard; A = Tetracycline (30 µg); B = Novobiocine (30 µg), Antifungal Standard; C = Clotrimazole (50 µg); D = Cyclohexamide (50 µg)

16a–j showed moderate to favorable activity against the tested pathogens.

Firstly, the 7-amino-6-cyano-2-((4-methoxyphenyl) amino)-*N*-phenyl-5-(aryl)pyrazolo[1,5-*a*]pyrimidine-3-carboxamide **14a–e** displayed good antibacterial results, moderate antifungal activity, and the activity depends on the aryl group at position five and aromatic amide at position three of pyrazolo[1,5-*a*]pyrimidine derivatives **14**. The presence of a dimethoxy group at positions two and five in the aryl group and *meta* methyl group in pyrazolo[1,5-*a*]pyrimidine **14e** & **14b** exhibited antibacterial activity with IZ ranged between 16–20 mm compared with Tetracycline 18 mm and Novobiocin 16 mm. Additionally, these two derivatives displayed moderate antifungal activity with IZs ranged between 15–17 mm in comparison with Clotrimazole (IZ = 23 mm) and Cycloheximide (IZ = 32 mm). Further, replacement *N*-phenyl by *N*-(4-chlorophenyl) exhibited equipotent in case of 5-(2,5-*di*-CH_3O-C_6H_3)pyrazolo[1,5-*a*]pyrimidine-3-carboxamide derivative **14j** with IZs ranged between 16–21 mm, while 5-(3-CH_3-C_6H_4)pyrazolo[1,5-*a*]pyrimidine-3-carboxamide derivative **14g** revealed slight decrease with IZs 16 mm, and 15 mm against *B. subtilis* and *E. Coli*, respectively. Additionally, it was found that the phenyl ring in pyrazolo[1,5-*a*]pyrimidine-3-carboxamide derivative **14d** had higher activity than the corresponding member incorporating chloro group as *N*-(4-chlorophenyl)-pyrazolo[1,5-*a*] pyrimidine-3-carboxamide derivative **14j** against *B. subtilis* strain. Moreover, replacement *N*-phenyl by *N*-(4-chlorophenyl) of 3-carboxamide group in pyrazolo[1,5-*a*]pyrimidine derivatives **14h** and **14j** demonstrated no activity against fungal strains. Besides, addition of the electron-withdrawn group as chlorine atom in pyrazolo[1,5-*a*]pyrimidine-3-carboxamide derivatives **14f** and **14g** displayed increased the activity with IZ values from zero to 18 and 15 mm, respectively.

Similarly, the azomethine of 5-amino-pyrazole derivatives **16a–j** showed variation in activity related to the different substituents in both two-aryl groups at positions

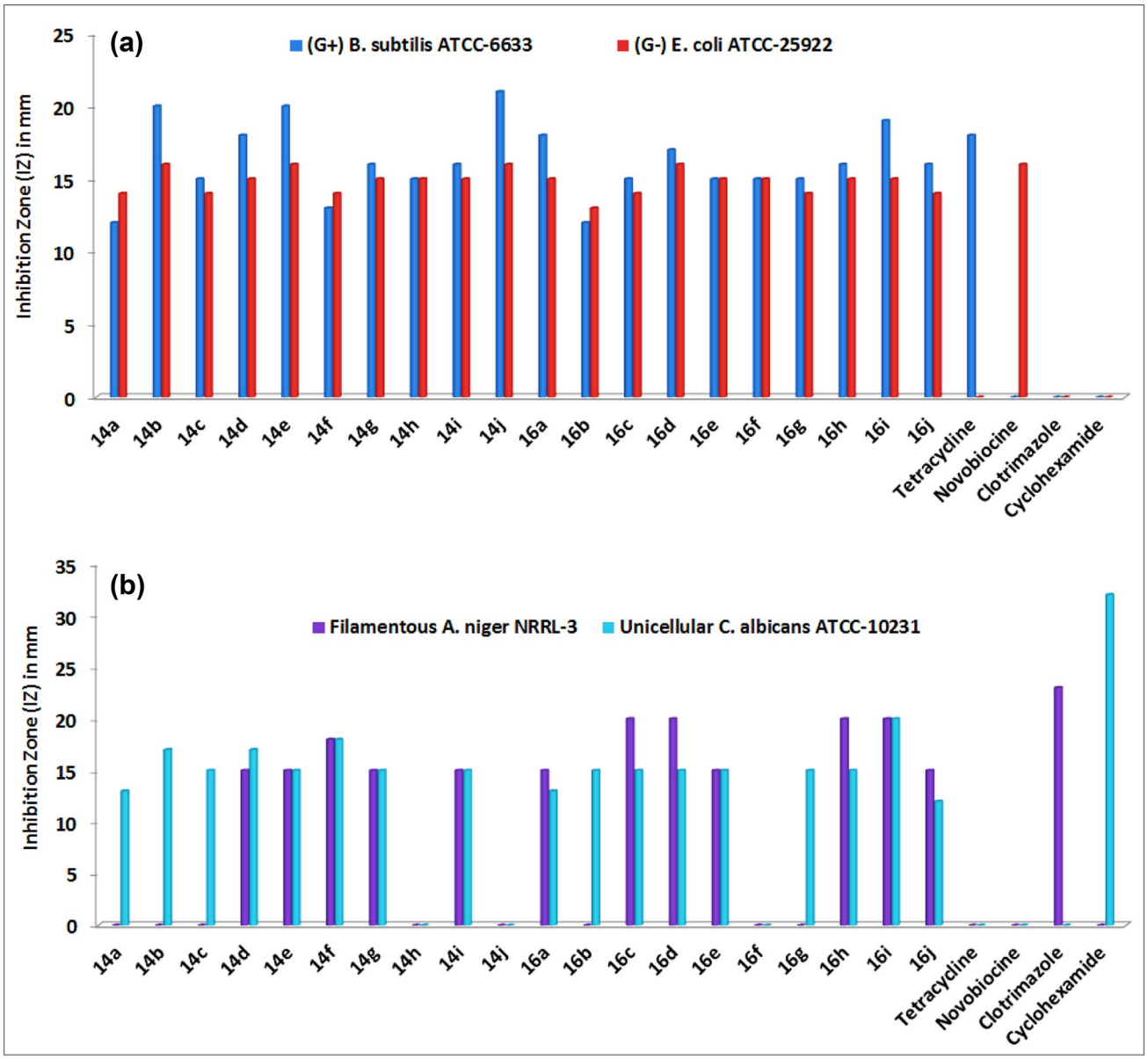

Fig. 3 Showed the antimicrobial activities (Inhibition Zone (IZ) in mm) of pyrazolo[1,5-*a*]pyrimidines **14a–j,** pyrazole Schiff bases **16a–j,** and standard antibiotics **a** bacteria, **b** fungi

three and five in pyrazole derivatives **16a–j**. Regarding the series of 5-((substituted benzylidene)amino)-1*H*-pyrazole-4-carboxamide derivatives **16a–j**, changing *N*-(phenyl) or *N*-(4-chlorophenyl) has little effect on antimicrobial activity. Furthermore, introducing more electron-withdrawing group as *N*-(4-chlorophenyl) to pyrazole derivatives **16a–j** increase activity against *B. subtilis* from 12–18 mm for pyrazoles **16a–e** to 15–19 mm for pyrazoles **16f–j**. Additionally, changing of 5-((substituted benzylidene)amino) by heterocyclic aldehyde as 5-((thiophen-2-ylmethylene)amino) in 1*H*-pyrazole-4-carboxamide derivatives **16a–d** and **16f–i** not cause significant enhancement in antimicrobial activity. The most active azomethine pyrazole derivatives **16a–j** among the synthesized derivatives that having 5-((4-chloro-3-nitrobenzylidene)amino) and *N*-(4-chlorophenyl)-4-carboxamide derivative is pyrazole derivative **16i** demonstrated antimicrobial activity IZs ranging between 15–19 mm and antifungal activity IZs 20 mm. Unfortunately, the pyrazole derivatives **16b**, **16f**, and **16g** are inactive against *A. Niger* except for moderate activity for other pyrazole derivatives. While the pyrazole derivative **16f** showed no activity against *C. albicans*.

Finally, in the general presence of the chloro atom in amide as *N*-(4-chlorophenyl) in position three in

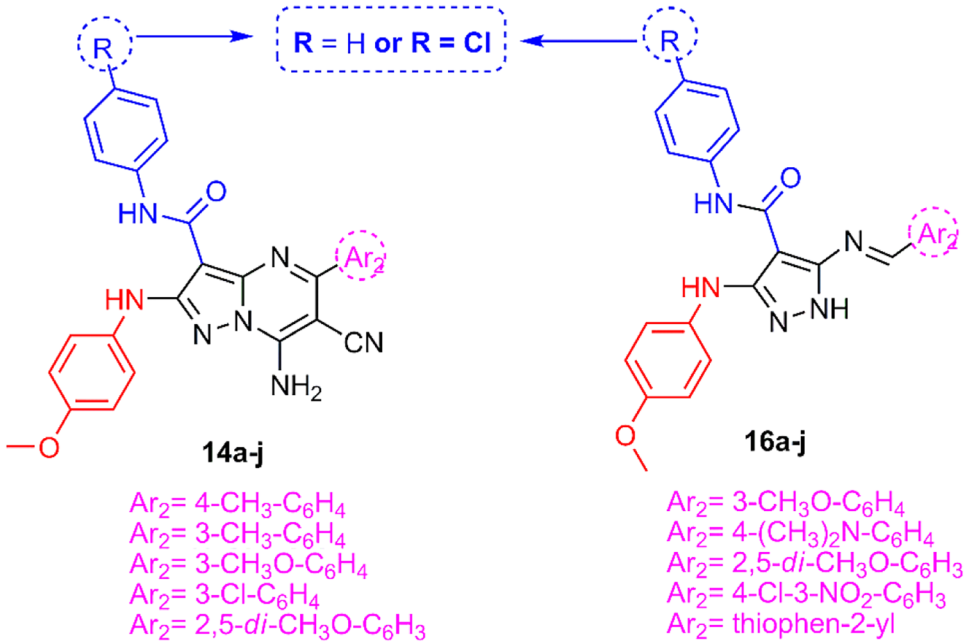

Fig. 4 Illustrate the structure of different substituent in both pyrazolo[1,5-*a*]pyrimidine derivatives **14a–j** and pyrazole-azomethine derivatives **16a–j**

pyrazolo[1,5-*a*]pyrimidine derivatives **14a–j** and position four in pyrazole derivatives **16a–j** causes increases the activity with significant results against *B. subtilis*, while in the case of *E. Coli* nearly results were obtained. Besides, *N*-(phenyl)-1*H*-pyrazolo[1,5-*a*]pyrimidin-3-carboxamide derivatives **14a–j** and *N*-(phenyl)-1*H*-pyrazole-4-carboxamide derivatives **16a–j** revealed abroad antifungal activity. Moreover, it can be concluded that the pyrazolo[1,5-*a*] pyrimidine derivatives **14a–j** more sensitive to antibacterial activity while 5-((substituted benzylidene)amino)-1*H*-pyrazole-4-carboxamide derivatives **16a–j** displayed better antifungal activity.

In silico studies

Physicochemical properties and drug-likeness model score

The physicochemical properties and drug-likeness (Lipinski and Veber rules) of the pyrazolo[1,5-*a*]pyrimidines (**14b**, **14e,** and **14j**) and Schiff bases (**16c**, **16d**, **16h,** and **16i**) were predicted by using the SwissADME web (http://swissadme.ch/index.php#undefined) [48, 49]. Also, the drug-likeness model score was predicted by using the Molsoft web (https://www.molsoft.com/mprop/) [50]. The predicted results are listed in Table 2.

From Table 2, the pyrazolo[1,5-*a*]pyrimidine **14b** and Schiff bases (**16c, 16d, 16h**, and **16i**) agreement with Lipinski's rule of five and with Veber's rule. While the two pyrazolo[1,5-*a*]pyrimidines (**14e** and **14j**) do not match with each of Lipinski's rule of five and Veber's rule by the violation in molecular weight and TPSA.

The rule for the drug-likeness model score estimation is based on positive and negative values, when the drug-likeness score was positive value; the compound was like a drug. But, if the drug-likeness score was negative value; the compound was non-drug [51].

Accordingly, all the tested compounds except **16c** showed positive values in the range from 0.05 to 0.44; therefore, these compounds may be considered to be drug-like. Figure 5 represents the drug-likeness model score of the two pyrazolo[1,5-*a*]pyrimidines **14b** and **14j**.

The bioactivity scores prediction

The bioactivity scores of the pyrazolo[1,5-*a*]pyrimidines (**14b**, **14e,** and **14j**) and Schiff bases (**16c**, **16d**, **16h,** and **16i**) toward G protein-coupled receptor (GPCR) ligand, ion channel modulator, a kinase inhibitor, nuclear receptor ligand, protease inhibitors, and enzyme inhibitor were predicted by using the Molinspiration bioactivity score v2018.03 web (https://www.molinspiration.com/cgi-bin/properties) [52]. The predicted results are written in Table 3.

The rule for the bioactivity scores estimation is the following: when the bioactivity score was more than 0.00; the compound was considered active. While if the bioactivity score in the range between − 0.50 and 0.00; the compound was moderately active. But if the bioactivity score was less than − 0.50, the compound was inactive.

The following observations are concluded from Table 3:

Table 2 Physicochemical properties and drug-likeness model score of the pyrazolo[1,5-*a*]pyrimidines (**14b**, **14e,** and **14j**) and pyrazole Schiff bases (**16c**, **16d**, **16h,** and **16i**)

Physicochemical properties and drug-likeness score	Pyrazolo[1,5-*a*]pyrimidines			Pyrazole Schiff bases			
	14b	**14e**	**14j**	**16c**	**16d**	**16h**	**16i**
Molecular weight ≤ 500	489.53	535.55	570.00	471.51	490.90	505.95	525.34
#H-bond acceptors ≤ 10	5	7	7	6	6	6	6
#H-bond donors ≤ 5	3	3	3	3	3	3	3
Lipophilicity MLOGP ≤ 4.15	3.26	2.46	2.92	3.03	3.28	3.50	3.75
Violations Lipinski's rule (Yes; 0 or 1)	Yes; 0	No; 2 MW > 500, N or O > 10	No; 2 MW > 500, N or O > 10	Yes; 0	Yes; 0	Yes; 1: MW > 500	Yes; 1: MW > 500
#Rotatable bonds ≤ 10	7	9	9	10	9	10	9
TPSA[a] ≤ 140	130.36	148.82	148.82	109.86	137.22	109.86	137.22
Violations Veber's rule (Yes; 0)	Yes; 0	No; 1: TPSA > 140	No; 1: TPSA > 140	Yes; 0	Yes; 0	Yes; 0	Yes; 0
Drug-likeness model score (MolSoft)	0.38	0.06	0.44	-0.23	0.05	0.22	0.15

[a]*TPSA* Topological polar surface area

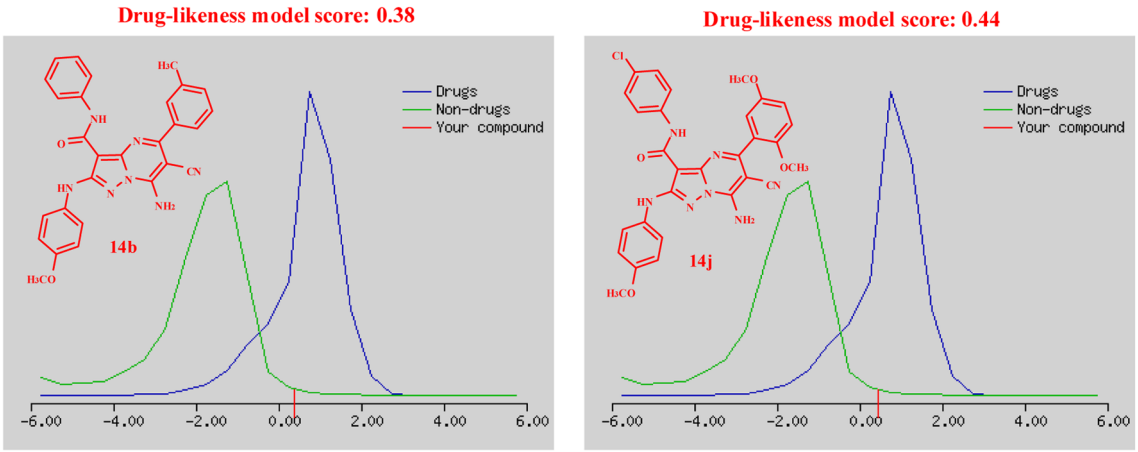

Fig. 5 Displayed the drug-likeness model score plotting of two pyrazolo[1,5-*a*]pyrimidines **14b** and **14j**. The green curve represents non-drug, and the blue curve represents drug

Table 3 The bioactivity scores prediction of the pyrazolo[1,5-*a*]pyrimidines (**14b**, **14e**, and **14j**) and pyrazole Schiff bases (**16c**, **16d**, **16h,** and **16i**)

The bioactivity scores	Pyrazolo[1,5-*a*]pyrimidines			Pyrazole Schiff bases			
	14b	**14e**	**14j**	**16c**	**16d**	**16h**	**16i**
GPCR ligand[a]	−0.11	−0.10	−0.12	−0.32	−0.44	−0.31	−0.43
Ion channel modulator	−0.32	−0.44	−0.52	−0.61	−0.60	−0.62	−0.61
Kinase inhibitor	0.45	0.36	0.30	0.07	−0.02	0.06	−0.03
Nuclear receptor ligand	−0.61	−0.62	−0.67	−0.60	−0.77	−0.59	−0.75
Protease inhibitor	−0.42	−0.39	−0.41	−0.37	−0.56	−0.39	−0.55
Enzyme inhibitor	−0.23	−0.26	−0.32	−0.28	−0.38	−0.29	−0.37

[a]G protein-coupled receptor (GPCR) ligand

- G protein-coupled receptor (GPCR) ligand: all the pyrazolo[1,5-*a*]pyrimidines (**14b**, **14e,** and **14j**) and Schiff bases (**16c**, **16d**, **16h,** and **16i**) were found to be moderately active with the bioactivity scores in the range from − 0.10 to − 0.44.
- Ion channel modulator: the two pyrazolo[1,5-*a*]pyrimidines **14b** and **14e** were found to be moderately active with the bioactivity scores − 0.32 and − 0.44, respectively, while the other compounds were found to be inactive.
- Kinase inhibitor: the three pyrazolo[1,5-*a*]pyrimidines (**14b**, **14e,** and **14j**) and the two Schiff bases (**16c** and **16h**) were found to be active with bioactivity scores in the range from 0.06 to 0.045. While the two Schiff bases (**16d** and **16i**) were found to be moderately active with the bioactivity scores − 0.02 and − 0.03, respectively.
- Nuclear receptor inhibitor: all the pyrazolo[1,5-*a*]pyrimidines (**14b**, **14e,** and **14j**) and Schiff bases (**16c**, **16d**, **16h,** and **16i**) were found to be inactive with the bioactivity scores less than − 0.50 (the range from − 0.59 to − 0.77).
- Protease inhibitor: the three pyrazolo[1,5-*a*]pyrimidines (**14b**, **14e,** and **14j**) and the two Schiff bases (**16c** and **16h**) were found to be moderately active (range from − 0.37 to − 0.42). But, the two Schiff bases (**16d** and **16i**) were found to be inactive with the bioactivity scores -0.56 and -0.55, respectively.
- Enzyme inhibitor: all the pyrazolo[1,5-*a*]pyrimidines (**14b**, **14e,** and **14j**) and Schiff bases (**16c**, **16d**, **16h,** and **16i**) were found to be moderately active (range from − 0.23 to − 0.38).

From the above, the pyrazolo[1,5-*a*]pyrimidine **14b** almost shows the highest bioactivity score compared to the other compounds.

ADME and toxicity properties prediction

ADME properties and toxicity properties prediction of the pyrazolo[1,5-*a*]pyrimidines (**14b**, **14e**, and **14j**) and Schiff bases (**16c**, **16d**, **16h,** and **16i**) were predicted by using the Pre-ADMET web (https://preadmet.bmdrc.kr/) [53]. The predicted results are written in Table 4.

The following observations are concluded from Table 4:

- Cytochrome P450 isoforms determine the pharmacokinetic properties, bioactivation, and safety persistence of drugs. In the case of all the pyrazolo[1,5-*a*]pyrimidines (**14b**, **14e,** and **14j**) and Schiff bases (**16c**, **16d**, **16h,** and **16i**) are an inhibitor of the two enzymes (CYP2C9 and

Table 4 ADME and toxicity properties prediction of the pyrazolo[1,5-*a*]pyrimidines (**14b**, **14e,** and **14j**) and pyrazole Schiff bases (**16c**, **16d**, **16h,** and **16i**)

ADME and toxicity properties prediction	Pre-ADMET web						
	Pyrazolo[1,5-a]pyrimidines			Pyrazole-Schiff bases			
	14b	14e	14j	16c	16d	16h	16i
CYP2C19 inhibition							
CYP2C9 inhibition							
CYP2D6 inhibition							
CYP3A4 inhibition							
P-glycoprotein inhibition							
Plasma Protein Binding	91.17	91.23	85.27	86.22	94.18	83.91	98.23
Ames test (Mutagenicity)							
Carcinogenicity (Mouse)							
Carcinogenicity (Rat)							
hERG inhibition							

= Inhibitor, Non-mutagen, Negative carcinogenicity, and low risk

= Non-inhibitor, Mutagen, Positive carcinogenicity, and high risk

= Ambiguous, = Medium risk

CYP3A4). But all the compounds are non-inhibitor of the two enzymes (CYP2C19 and CYP2D6).

- P-glycoprotein (P-gp) has two functions the first is a barrier for delivering drugs properly and it is responsible for extruding toxins. All the compounds (**14b**, **14e**, **14j**, **16c**, **16d**, **16h,** and **16i**) were found to be effective.
- The rule for the plasma protein binding (PPB) estimation is the following: when the value was less than 90%; the compound was low activity. While if the value was more than or equal to 90%; the compound was high activity. The two pyrazolo[1,5-*a*]pyrimidines (**14b** and **14e**) and two Schiff bases (**16d** and **16i**) had plasma protein binding (PPB) more than 90% (range from 91.17 to 98.23%, highly active), which affects the excretion of the drugs and its efficiency.
- Ames test (mutagenicity), the three pyrazolo[1,5-*a*]pyrimidines (**14b**, **14e**, and **14j**) and three Schiff bases (**16c**, **16d**, and **16h**) were predicted to be mutagens.
- Carcinogenicity (mouse) test and the two Schiff bases (**16d** and **16i**) were predicted as positive, while the three pyrazolo[1,5-*a*]pyrimidines (**14b**, **14e**, and **14j**) and the two Schiff bases (**16c** and **16h**) presented negatively.
- Carcinogenicity (rat) test, the pyrazolo[1,5-*a*]pyrimidine **14j,** and the three Schiff bases (**16d**, **16h,** and **16i**) were predicted as negative.
- In the case of the hERG inhibition, the two compounds **14e** and **16c** showed high risk and the three compounds **14j**, **16h**, and **16i** presented a medium risk. While compounds **14b** and **16d** presented an ambiguous risk.

From the above, all compounds are an inhibitor of the two cytochrome P450 isoforms (CYP2C9 and CYP3A4 enzymes) and P-glycoprotein (P-gp). Besides, some compounds showed highly active toward plasma protein binding (PPB), were predicted as negative against Carcinogenicity (mouse and rat) test, and presented medium risk in the case of the hERG inhibition.

Computational study of the binding mode

One of the most important tools in structure-based drug discovery is molecular docking simulation. It can describe newly designed derivatives' behavior in the binding site of target proteins [54]. Docking study plays an important role and considers one of the most applied simulated screening methods due to its ability to predict and get insights into a protein–ligand complex structure, which is useful information for the successful development of drug targeting and lead optimization [55]. The preferring structure selected from one to another in the docking study related to the highest binding affinity between the ligand and the protein [56]. Our study involved simulation of the most active derivatives inside both DNA gyrase for bacterial and secreted aspartic protease for fungal promising derivatives using Molecular Operating Environmental (MOE) software version 2008.10. The docking result is represented in Table 5 and Fig. 6a–d.

Study the most active derivatives against bacterial strains inside DNA gyrase

The most active derivatives **14b**, **14e**, **14j**, and **16i** against *Bacillus subtilis* and *Escherichia coli* were docked inside the active site of *S. auras* DNA gyrase (PDB: 2XCT) [57, 58]. The co-crystallized ligand (Ciprofloxacin) redocked inside *S. aureus* Gyrase's active site revealed binding energy $S = -9.87$ kcal mol^{-1}. The ligand formed one hydrogen bond donor between Tyr580 and nitrogen of piperazine ring as well as hydrogen bond acceptor between His1081 and oxygen of carboxylate group with bond length 2.35, 2.30 Å, respectively. The most promising pyrazolo[1,5-*a*]pyrimidine-3-carboxamide derivative **14j** with inhibition zone (IZ) ranged between 16-21 mm showed binding energy $S = -25.35$ kcal mol^{-1}, through two hydrogen bond and one arene–cation interaction between His1061 and pyrazole ring. The residue Asp512 formed a side-chain hydrogen bond donor with the amino group of pyrimidine as well as a side-chain hydrogen bond acceptor between Ser1028 and oxygen of methoxy group with bond length and strength 2.83 Å (11%), 2.99 Å (38%), respectively Fig. 6a.

Furthermore, *N*-phenyl-5-(3-methylphenyl)pyrazolo[1,5-*a*]pyrimidine-3-carboxamide derivative **14b** exhibited binding affinity $S = -23.05$ kcal mol^{-1}, through two hydrogen bonds from a side-chain. These two bonds created between the Ser1028 with the cyano in pyrimidine ring (H-acceptor), Ser1028 with the amino of pyrimidine (H-donor) with bond length 2.89 Å, and 3.05 Å. Besides, arene–cation interaction between His1061 and pyrazole ring Fig. 6b. Similarly, *N*-phenyl-5-(2,5-dimethoxyphenyl)-pyrazolo[1,5-*a*]pyrimidine-3-carboxamide derivative **14e** displayed binding energy $S = -22.76$ kcal mol^{-1}, by one hydrogen bond side-chain acceptor between Ser1028 and cyano group attached to pyrimidine ring as well as one arene–cation interaction between His1061 and pyrazole ring. Moreover, *N*-(4-chlorophenyl)-1*H*-pyrazole-4-carboxamide **16i** displayed one hydrogen bond donor between Asp510 and NH of pyrazole ring with bond length 2.76 Å and strength 45%.

Finally, the active derivatives **14b**, **14e**, **14j**, and **16i** showed a good binding affinity inside the pocket sites of DNA gyrase ranged between −25.35 to −20.18 kcal mol^{-1} with different binding modes and therefore suggested that these derivatives act as gyrase inhibitors.

Table 5 Molecular modeling study of the most promising derivatives inside the active sites of *S. aureus* DNA gyrase (PDB: 2XCT) and secreted aspartic protease from *c. albicans* (PDB: IZAP)

Cpd. No	*S* (kcal mol^{-1})	Residue	Interacting groups	Distance (Å)	Strength (%)	Hydrophobic interaction
Docking inside the *S. aureus* DNA gyrase (PDB: 2XCT)						
14b	− 23.05	Ser1028	CN of pyrimidine	2.89	57	Arg1033, Val511, Ala1032, Asp510, Asp512, Glu435, Tyr1150, Pro1080, Tyr580, Lys581
		Ser1028	NH2 of pyrimidine	3.05	15	
		His1061	Pyrazole ring	–	–	
14e	− 22.76	Ser1028	CN OF Pyrimidine	2.88	69	Arg1033, Val511, Asp512, Asp510, Pro1080, Lys581, Tyr1150, Tyr580, Gly582, Lys581
		His1061	Pyrazole ring	–	–	
14j	− 25.35	Asp512	NH2 of pyrimidine	2.59	50	Asp508, Asp510, Lys581, Pro1080, Gly582, Glu585
		Ser1028	Oxygen of methoxy			
		His1061	Pyrazole ring			
16i	− 20.18	Asp510	NH of pyrazole	2.76	45	Ser438, Asp437, Gly436, Glu435, Gly582, Lys581, Gly545, Tyr580, Tyr1150
Cip	− 9.87	His1081	Oxygen of carboxylate	2.30	37	Ser1028, Arg1033, Val511, Asp510, Pro1080, Tyr1150, Lys581, Gly545
		Tyr580	Nitrogen of piprazine	2.35	48	
Docking inside the secreted aspartic protease from *c. albicans* (PDB: IZAP)						
16c	− 27.52	Asp218	NH of anisidine der	2.41	37	Tyr225, Gly85, Thr221, Iie305, Gly220, Tyr84, Asn301, Leu216, Glu193, Gly34, Thr13, Ile30, Ile119
		Asp32	Nitrogen of pyrazole	2.72	28	
		Ser88	Oxygen of methoxy gr	3.20	16	
16d	− 24.91	Gly34	NH of anisidine der	2.97	22	Gly83, Thr221, Glu193, Ala303, Gly85, Asp86, Ile305, Asn301
		Asp218	NH of pyrazole	2.56	27	
		Arg195	Phenyl of benzamide	–	–	
		Tyr225	Aryl of aldehyde der	– –	– –	
16h	− 27.66	Asp32	Nitrogen of pyrazole	2.84	24	Gly34, Leu216, Asn301, Thr221, Ile305, Tyr225, Ile119, Ile30, Thrr84, Asp86, Val12, Ser88, Asp32, Gly85
		Asp32	Nitrogen of pyrazole	2.80	12	
		Asp218	NH of anisidine der	2.41	39	
16i	− 28.03	Asn301	Oxygen of methoxy	3.18	13	Tyr225, Ile305, Gly85, Asp86, Asp218, Ser35, Gly34, Asn131, Asp32, Thr221, Gly220, Gly83, Glu132, Ile82, Ile133
		Tyr84	Aryl of benzamide der	–	–	
L.Nor	− 30.98	Thr221	NH of amide der	3.05	22	Ile223, Tyr84, Leu216, Asp86, Gly220, Glu193, Asp32, Ile123, Ala303, Gly85, Ile305, Asn301, Tyr225, Thr222
		Asp218	OH group	2.31	23	

Cip. = Ciprofloxacin; L.Nor. = Norleucinamide; (–) arene–cation interaction, (– –) arene–arene interaction

Study the most active derivatives against fungal strains inside secreted aspartic protease

As new possible antifungal drug goals, secreted aspartic protease (Saps) obviously hold promise. Saps are important virulence factors because it includes a wide variety of physiological processes of fungal as well as the various aspects of the interactions between host and fungal [59]. Similarly, the most active four pyrazole derivatives **16c**, **16d**, **16h**, and **16i** against *A. niger* and *C. albicans* were docked inside the active site of secreted aspartic protease (Saps) (PDB: 1ZAP) [58]. The co-crystallized ligand (L-Norleucinamide derivative) showed binding energy $S = -30.98$ kcal mol^{-1} through two hydrogen bond side-chain donor between the residue Thr221 and NH of amide derivative as well as Asp218 with hydroxyl group with bond length 3.05 Å (22%) and 2.31 Å (23%), respectively. The most promising derivative against fungal strains 1*H*-pyrazole-4-carboxamide derivative **16i** exhibited binding energy $S = -28.03$ kcal mol^{-1} through one side-chain hydrogen bond acceptor. The pyrazole derivative **16i** indicated that a hydrogen bond was formed between the oxygen of the methoxy group and the residue Asn301 (distance 3.18 Å and strength 13%). Meanwhile, an arene–arene interaction was observed between the 4-chlorobenzamide derivative and Tyr84 (Fig. 6c). (All docking study figures in supplementary material, Figures S3-S22).

Additionally, the NH of pyrazole and NH of anisidine derivatives in pyrazole **16d** could form two hydrogen bonds donor between Asp218 and Gly34, respectively. Besides, the aryl group of aldehyde derivative created an arene–cation interaction with Tyr225. Further, the docking pose of 5-((2,5-dimethoxybenzylidene)amino)-3-((4-methoxyphenyl)amino)-*N*-(4-chlorophenyl)-1*H*-pyrazole-4-carboxamide (**16h**) demonstrated three favorable

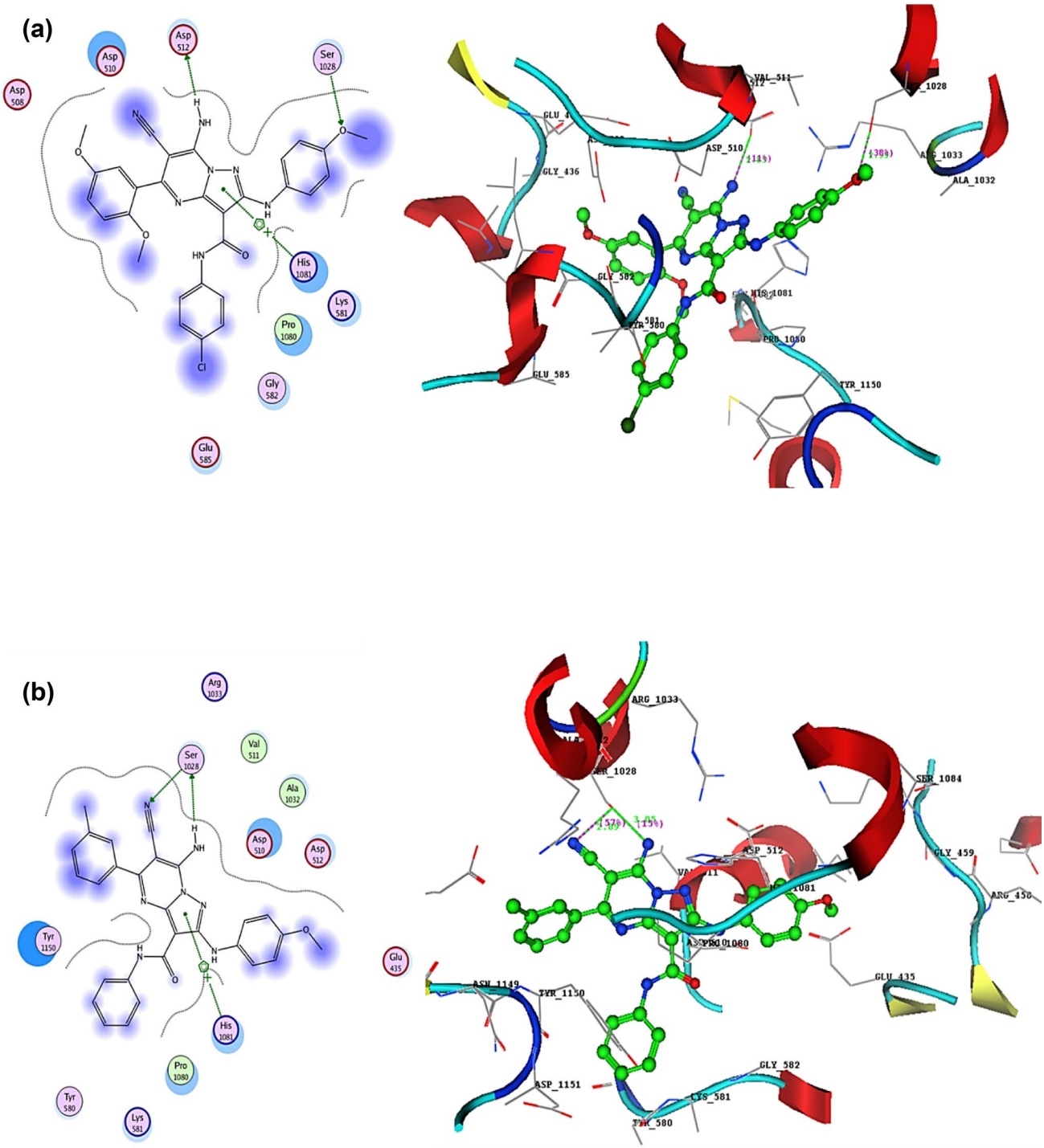

Fig. 6 **a** 2D and 3D binding mode of pyrazolo[1,5-*a*]pyrimidine-3-carboxamide derivative **14j** inside the active site of *S. auras* DNA gyrase (PDB: 2XCT). **b** 2D and 3D binding mode of pyrazolo[1,5-*a*]pyrimidine-3-carboxamide derivative **14b** inside the active site of *S. auras* DNA gyrase (PDB: 2XCT). **c** 2D and 3D binding mode of 1*H*-pyrazole-4-carboxamide derivative **16i** inside the active site of secreted aspartic protease (Saps) (PDB: 1ZAP). **d** 2D and 3D binding mode of 1*H*-pyrazole-4-carboxamide derivative **16c** inside the active site of secreted aspartic protease (Saps) (PDB: 1ZAP)

hydrogen bonds with binding energy $S = -27.66$ kcal mol^{-1}. Two of them between the nitrogen of pyrazole derivative with the oxygen of carboxylate and oxygen of carbonyl of Asp32 (distance 2.81, 2.84 Å). Besides, one hydrogen bond side-chain donor between the NH of anisidine moiety and Asp218 with bond length 2.41 Å. Furthermore,

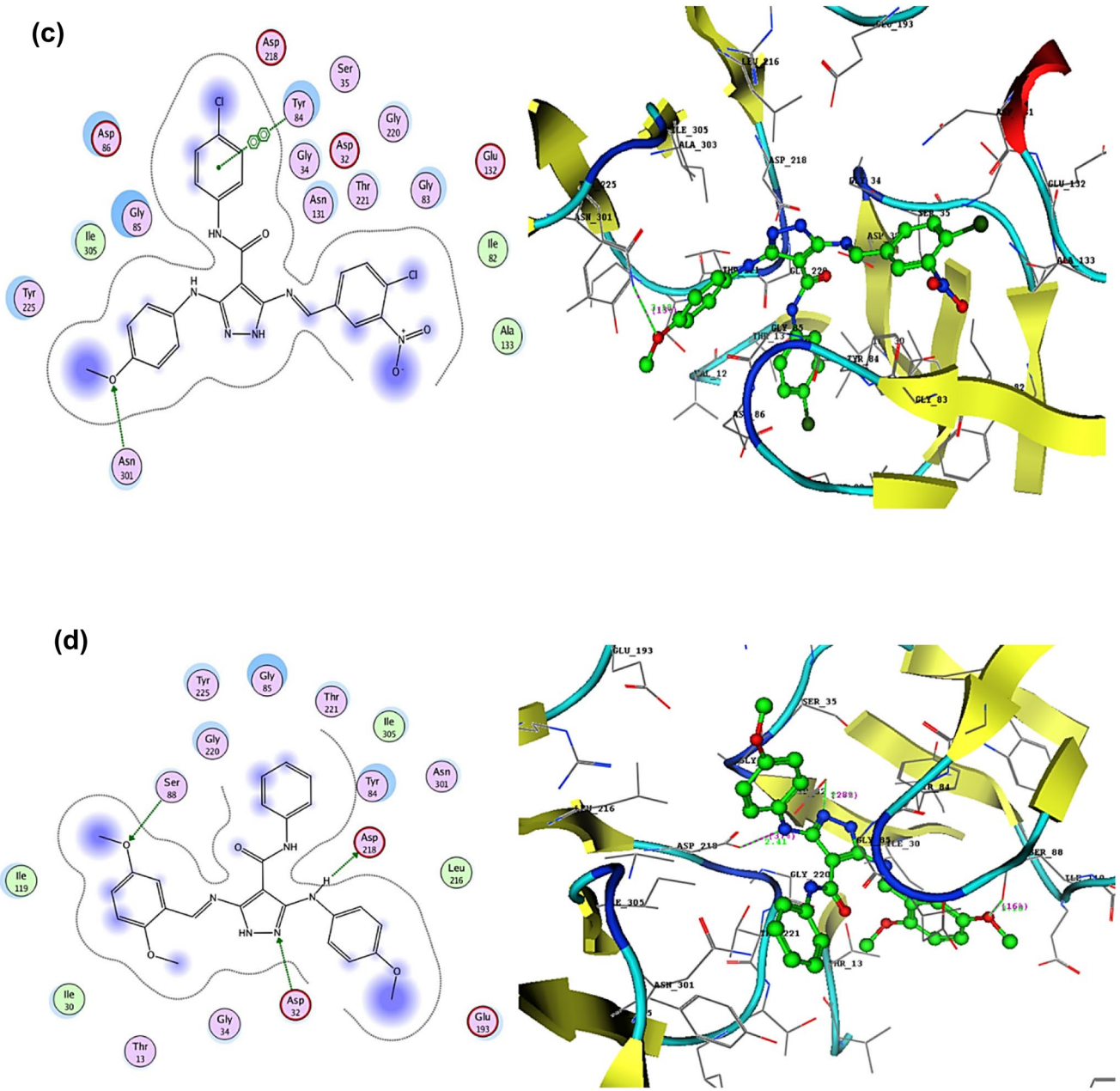

Fig. 6 (continued)

N-phenyl-1*H*-pyrazole-4-carboxamide **16c** displayed binding energy $S = -27.52$ kcal mol^{-1} with three hydrogen bonds between Asp218, Asp32, and Ser88 with NH of anisidine, the nitrogen of pyrazole, and oxygen of methoxy group, respectively (Fig. 6d). (All docking study figures in supplementary material, Figures S3-S22).

Finally, it can be concluded that the docking results revealed that the 1*H*-pyrazole-4-carboxamide derivative **16c**, **16d**, **16h**, and **16i** binding to the active site of secreted aspartic protease (Saps) (PDB: 1ZAP) and may act as inhibitors. Besides, the other derivatives **14b**, **14e**, **14j**, and **16i** were suggested to be DNA gyrase inhibitors with good bind energy scores and different binding modes. Overall, these derivatives are suggested to be inhibitors for bacterial and fungal by a different mode of actions and thus may participate in antimicrobial activity.

Molecular electrostatic potential (MEP) maps

Our work was extended to investigate the reasons behind a good binding of the most promising derivatives inside the two active pockets. Molecular electrostatic potential (MEP)

maps were generated to determine the charge distribution around a molecule. MEP maps provide information about the regions with electron-rich regions (red) and electron deficiency regions, i.e., hydrophobic regions that responsible for forming interactions (hydrogen bonds, arene–arene, and arene–cation interactions) with the residue inside the active site. The MEP was performed using MOE 2008.10, where the active derivatives' geometry optimized using the MMFF94x force field according to the previously reported method [60]. As represented in Fig. 7, the positive charge (blue) was located on the nitrogen of pyrimidine and pyrazoles as well as amino, cyano, and NH of both benzamide and anisidine derivatives. Simultaneously, the negative charge (red) was displayed on the oxygen of carbonyl and methoxy groups. Finally, the presence of nucleophiles (red) and electrophile (blue) regions showed that these regions could form hydrogen bonding donors and acceptors and illustrate the binding mode in the docking study (All Molecular Electrostatic Potential (MEP) maps figures in supplementary material, Figures S23-S29).

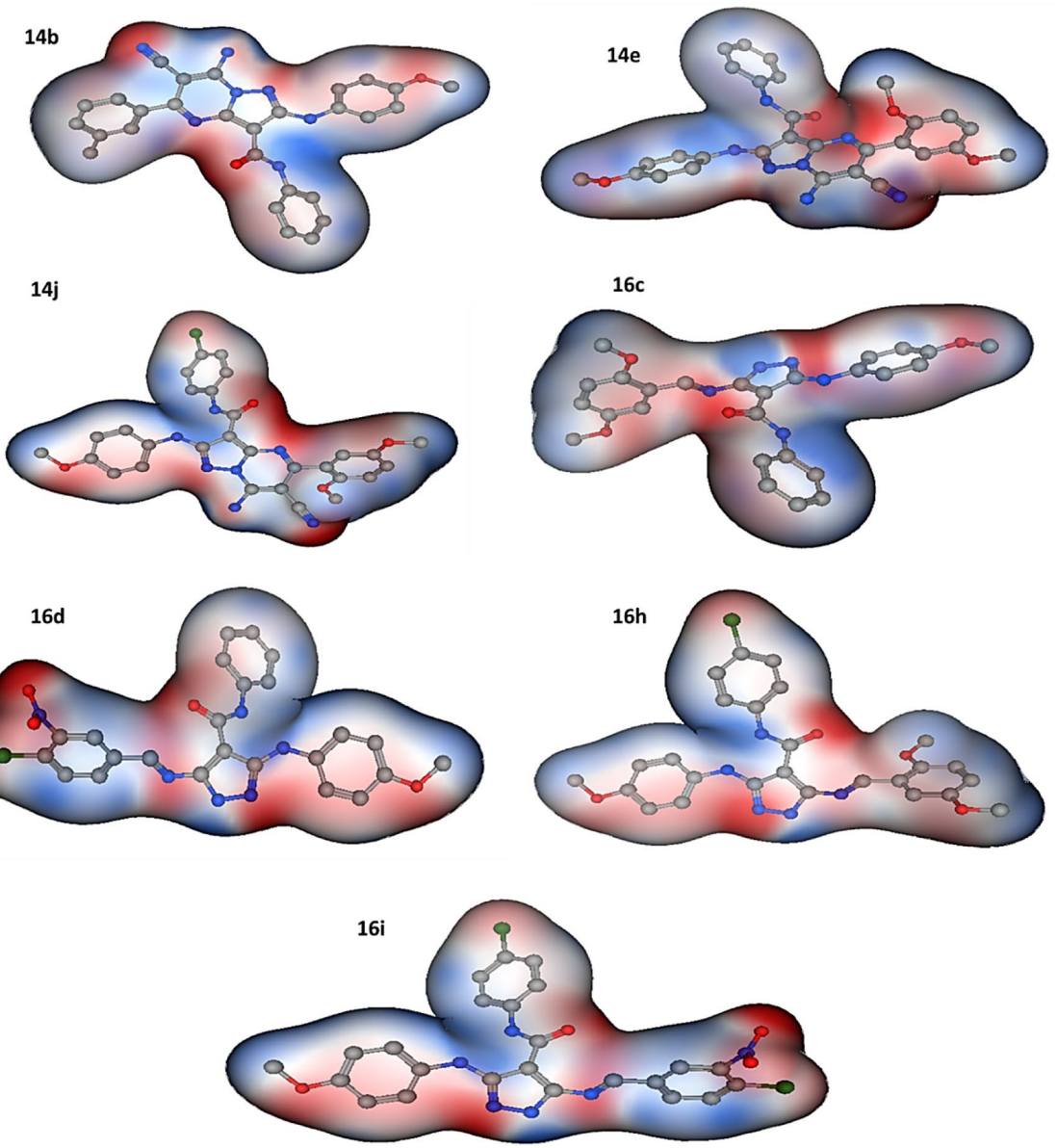

Fig. 7 Showed molecular electrostatic potential maps of most promising derivatives to determine the charge distribution around molecules

Conclusion

In summary, new bioactive pyrazolo[1,5-*a*]pyrimidines **14a–j** and pyrazole Schiff bases **16a–j** have been designed and synthesized by the reaction of 5-amino-pyrazoles **9a**, **b** with 2-(arylidene)malononitriles **10a–e** or various aldehydes **15a–e**, respectively. The structures of new bioactive pyrazolo[1,5-*a*]pyrimidines **14a–j** and pyrazole Schiff bases **16a–j** were confirmed using different spectroscopic techniques. The pyrazolo[1,5-*a*]pyrimidines **14a–j** and pyrazole Schiff bases **16a–j** were screened for their in vitro antimicrobial activities against four microbes. The three pyrazolo[1,5-*a*]pyrimidines (**14b**, **14e,** and **14j**) and four pyrazole Schiff bases (**16c**, **16d**, **16h,** and **16i**) proved to be potent against the four microbes tested, have a wide spectrum effect, and in several cases, their activities exceeded that of the reference drugs used. The structure–activity relationship (SAR) was performed. As well as, physicochemical properties, drug-likeness model score, bioactivity scores, ADME, and toxicity properties were predicted in silico. The prediction result showed the five compounds (**14b, 16c, 16d, 16h**, and **16i**) agreement with Lipinski's rule of five and with Veber's rule. Also, in the case of a drug-likeness model score, all the tested compounds (**14b**, **14e, 14j**, **16d**, **16h,** and **16i**) except **16c** showed positive values (range 0.05 to 0.44). Therefore, these compounds may be considered to be drug-like. The pyrazolo[1,5-*a*] pyrimidine **14b** almost shows the highest bioactivity score compared to the other compounds. All compounds are an inhibitor of CYP2C9, CYP3A4 enzymes, and P-glycoprotein (P-gp). Also, some compounds showed highly active ($\geq 90\%$) toward plasma protein binding (PPB), were predicted as negative against carcinogenicity (mouse and rat) test, and presented medium risk in the hERG inhibition test. Furthermore, molecular docking studies were performed for the most active derivatives against *S. auras* DNA gyrase (PDB: 2XCT) and secreted aspartic protease (Saps) (PDB: 1ZAP) as antibacterial and antifungal targets, respectively, to determine the binding patterns. The most active antibacterial derivatives **14b**, **14e**, **14j**, and **16i** against DNA Gyrase (PDB:2XCT) showed binding energy $S = -25.35$ to -20.18 kcal mol^{-1}. Besides, for promising fungal derivatives **16c**, **16d**, **16h**, and **16i** displayed binding energy $S = -28.03$ to -24.91 kcal mol^{-1}, and both of them showed different types of binding mode. The results suggested that these derivatives could act as good antimicrobial agents. MEP maps were performed to provide information about the regions with electron-rich regions (red) and electron deficiency regions that responsible for forming interactions with the residue inside the active site and therefore confirmed the binding mode in the docking study. In the future, these compounds are possibly suitable temples for the development of a novel antibacterial and antifungal therapeutic drug.

Materials and methods

Chemistry

All melting points were measured on a Gallenkamp melting point apparatus and are uncorrected. The IR spectra were recorded (KBr disk) on a PerkinElmer 1650 FTIR instrument. ^{1}H NMR (500 or 400 MHz) and ^{13}C NMR (125 or 100 MHz) spectra were recorded on a JEOL spectrometer using DMSO-d_6 as solvent and tetramethylsilane (TMS) as an internal standard. Chemical shifts (δ-values) are reported in ppm. Mass spectra were recorded on a Varian MAT 112 spectrometer at 70 eV. Elemental analyses were performed at the Micro Analytical Center, Cairo University, Egypt.

The progress of the reactions was monitored by thin-layer chromatography (TLC) using aluminum sheets coated with silica gel F_{254} (Merck), viewing under a short-wavelength UV lamp effected detection. All evaporations were performed under reduced pressure at 40 °C.

3-Methoxybenzaldehyde (**15a**), 4-(dimethylamino)benzaldehyde (**15b**), 2,5-dimethoxybenzaldehyde (**15c**), 4-chloro-3-nitrobenzaldehyde (**15d**), and thiophene-2-carbaldehyde (**15e**) were of Merck AR grade, Germany.

Synthesis of 5-amino-N-aryl-3-(4-methoxyphenylamino)-1H-pyrazole-4-carboxamide (**9a, b**) [41] and *2-(arylidene) malononitriles* (**10a–e**) [42, 43] were prepared according to the literature procedure.

Synthesis of 7-amino-6-cyano-5-aryl-2-(4-methoxyphenyl amino)-*N*-aryl-pyrazolo[1,5-*a*]pyrimidine-3-carboxamides (14a–j)

A mixture of 5-amino-*N*-aryl-1*H*-pyrazole-4-carboxamide derivatives **9a**, **b** (0.01 mol) with 2-(arylidene)malononitriles **10a–e** (0.01 mol) as [2-(4-methylbenzylidene)malononitrile (**10a**), 2-(3-methylbenzylidene)malononitrile (**10b**), 2-(3-methyoxybenzylidene)malononitrile (**10c**), 2-(3-chlorobenzylidene)malononitrile (**10d**), and 2-(2,5-dimethoxybenzylidene)malononitrile (**10e**)] and a catalytic amount of triethylamine (four drops) in absolute ethanol (30 mL) was refluxed for 6 h. After cooling, the solvent was concentrated under reduced pressure and the solid obtained was collected and recrystallized from ethanol to give the corresponding pyrazolo[1,5-*a*]pyrimidines **14a–j**.

7-Amino-6-cyano-2-(4-methoxyphenylamino)-*N*-phenyl-5-(4-methylphenyl)pyrazolo[1,5-*a*]pyrimidine-3-carboxamide (14a)

Yellow crystals; M.p.: > 300 °C; Yield (80%); IR (KBr) ν_{max}/cm^{-1} 3428, 3304 (NH_2, 2NH), 2213 (C≡N), 1641 (C=O), 1597 (C=N), 1551 (C=C); ^{1}H NMR (500 MHz, DMSO-d_6, δ/ppm): 2.43 (s, 3H, CH_3), 3.74 (s, 3H, OCH_3), 6.90 (d, 2H, J = 9.0 Hz, *p*-methoxyphenyl ring), 7.09 (t, 1H, J = 7.5 Hz, phenyl ring), 7.37 (t, 2H, J = 7.8 Hz, phenyl ring), 7.44 (d, 2H, J = 8.2 Hz, *p*-methylphenyl ring), 7.60 (d, 2H, J = 7.7 Hz, phenyl ring), 7.84 (d, 2H, J = 9.0 Hz, *p*-methoxyphenyl ring), 7.90 (d, 2H, J = 8.2 Hz, *p*-methylphenyl ring), 9.00 (s, *br*, 2H, NH_2 exchangeable by D_2O), 9.23, 10.14 (2s, 2H, 2NH exchangeable by D_2O); ^{13}C NMR (125 MHz, DMSO-d_6, δ ppm): 21.15 (C, CH_3), 55.26 (C, OCH_3), 74.88, 89.09, 114.26, 118.87, 119.06, 123.54, 123.78, 128.69, 129.24, 129.34, 133.40, 133.98, 138.46, 141.08, 145.70, 149.49, 153.98, 156.32, 161.47, 162.29 (26C); MS (*m/z*, %): 489 (M^+, 17.65%), 396 (base peak, 100%); Anal. Calcd. (%) for $C_{28}H_{23}N_7O_2$ (489.53): C, 68.70; H, 4.74; N, 20.03. Found: C, 68.98; H, 4.57; N, 20.29%.

7-Amino-6-cyano-2-(4-methoxyphenylamino)-*N*-phenyl-5-(3-methylphenyl)pyrazolo[1,5-*a*]pyrimidine-3-carboxamide (14b)

Yellow crystals; M.p.: > 300 °C; Yield (77%); IR (KBr) ν_{max}/cm^{-1} 3428, 3319 (NH_2, 2NH), 2216 (C≡N), 1656 (C=O), 1599 (C=N), 1554 (C=C); ^{1}H NMR (500 MHz, DMSO-d_6, δ/ppm): 2.48 (s, 3H, CH_3), 3.79 (s, 3H, OCH_3), 6.94 (d, 2H, J = 9.5 Hz, *p*-methoxyphenyl ring), 7.13 (d, 1H, J = 7.7 Hz, *m*-methylphenyl ring), 7.39 (t, 2H, J = 8.2 Hz, phenyl ring), 7.50 (d, 1H, J = 7.9 Hz, *m*-methylphenyl ring), 7.56 (t, 1H, J = 7.9 Hz, phenyl ring), 7.62 (d, 4H, J = 8.6 Hz, *m*-methylphenyl ring + phenyl ring), 7.86 (d, 2H, J = 9.2 Hz, *p*-methoxyphenyl ring), 9.12 (s, *br*, 2H, NH_2 exchangeable by D_2O), 9.23, 10.21 (2s, 2H, 2NH exchangeable by D_2O); Anal. Calcd. (%) for $C_{28}H_{23}N_7O_2$ (489.53): C, 68.70; H, 4.74; N, 20.03. Found: C, 68.53; H, 4.48; N, 20.27%.

7-Amino-6-cyano-5-(3-methoxyphenyl)-2-(4-methoxyphenylamino)-*N*-phenylpyrazolo[1,5-*a*]pyrimidine-3-carboxamide (14c)

Yellow crystals; M.p.: 258–260 °C; Yield (72%); IR (KBr) ν_{max}/cm^{-1} 3433, 3332 (NH_2, 2NH), 2212 (C≡N), 1652 (C=O), 1595 (C=N), 1547 (C=C); ^{1}H NMR (500 MHz, DMSO-d_6, δ/ppm): 3.74, 3.86 (2s, 6H, $2OCH_3$), 6.90 (d, 2H, J = 9.0 Hz, *p*-methoxyphenyl ring), 7.09 (t, 1H, J = 7.4 Hz, phenyl ring), 7.18–7.21 (m, 1H, *m*-methoxyphenyl ring), 7.36 (t, 2H, J = 7.9 Hz, phenyl ring), 7.54–7.56 (m, 3H, *m*-methoxyphenyl ring), 7.59 (d, 2H, J = 7.7 Hz, phenyl ring), 7.85 (d, 2H, J = 9.0 Hz, *p*-methoxyphenyl ring), 9.09 (s, *br*, 2H, NH_2 exchangeable by D_2O), 9.23, 10.14 (2s, 2H, 2NH exchangeable by D_2O); ^{13}C NMR (125 MHz, DMSO-d_6, δ/ppm): 55.43, 56.11 (2C, $2OCH_3$), 75.09, 89.19, 113.86, 114.24, 115.98, 116.90, 118.89, 119.06, 120.98, 123.51, 129.14, 129.87, 133.30, 137.95, 138.38, 145.57, 149.40, 154.00, 156.36, 159.26, 160.78, 162.17 (26C); MS (*m/z*, %): 505 (M^+, 41.43%), 93 (base peak, 100%); Anal. Calcd. (%) for $C_{28}H_{23}N_7O_3$ (505.53): C, 66.52; H, 4.59; N, 19.39. Found: C, 66.40; H, 4.31; N, 19.65%.

7-Amino-5-(3-chlorophenyl)-6-cyano-2-(4-methoxyphenylamino)-*N*-phenylpyrazolo[1,5-*a*]pyrimidine-3-carboxamide (14d) [61]

Orange crystals; M.p. > 300 °C; Yield (74%); IR (KBr) ν_{max}/cm^{-1} 3442, 3299 (NH_2, 2NH), 2212 (C≡N), 1665 (C=O), 1632 (C=N), 1598 (C=C); ^{1}H NMR (400 MHz, DMSO-d_6, δ/ppm) 3.78 (s, 3H, OCH_3), 6.89 (d, 2H, J = 9.0 Hz, *p*-methoxyphenyl ring), 7.07 (t, 1H, J = 7.4 Hz, phenyl ring), 7.33 (t, 2H, J = 8.3 & 7.5 Hz, phenyl ring), 7.60 (d, 2H, J = 8.0 Hz, phenyl ring), 7.62 (d, 1H, J = 2.9 Hz, *m*-chlorophenyl ring), 7.76 (d, 2H, J = 9.0 Hz, *p*-methoxyphenyl ring), 7.93–7.96 (m, 1H, *m*-chlorophenyl ring), 8.02 (s, 1H, *m*-chlorophenyl ring), 8.06 (d, 1H, J = 2.8 Hz, *m*-chlorophenyl ring), 8.93 (s, *br*, 2H, NH_2 exchangeable by D_2O), 9.28, 10.06 (2s, 2H, 2NH exchangeable by D_2O); ^{13}C NMR (100 MHz, DMSO-d_6, $CDCl_3$, δ/ppm): 55.45 (1C, OCH_3), 75.14, 89.98, 114.40, 115.97, 119.20, 119.29, 123.66, 127.23, 128.77, 129.21, 130.48, 130.86, 133.59, 134.16, 138.73, 138.78, 145.75, 149.60, 154.38, 157.00, 159.45, 162.53 (26C); MS (*m/z*, %): 511 (M^{+2}, 2.69), 509 (M^+, 8.45), 368 (base peak, 100%); Anal. Calcd. (%) for $C_{27}H_{20}ClN_7O_2$ (509.95): C, 63.59; H, 3.95; N, 19.23. Found: C, 63.50; H, 4.00; N, 19.27%.

7-Amino-6-cyano-5-(2,5-dimethoxyphenyl)-2-(4-methoxyphenylamino)-*N*-phenylpyrazolo[1,5-*a*]pyrimidine-3-carboxamide (14e)

Orange crystals; M.p. 210–212 °C; Yield (75%); IR (KBr) ν_{max}/cm^{-1} 3429, 3321 (NH_2, 2NH), 2217 (C≡N), 1654 (C=O), 1595 (C=N), 1552 (C=C); ^{1}H NMR (500 MHz, DMSO-d_6, δ/ppm): 3.72, 3.82, 3.88 (3s, 9H, $3OCH_3$), 6.90 (d, 2H, J = 7.5 Hz, *p*-methoxyphenyl ring), 7.07–7.22 (m, 4H, 2,5-dimethoxyphenyl ring + phenyl ring), 7.34 (t, 2H, J = 7.3 Hz, phenyl ring), 7.51 (d, 1H, J = 7.8 Hz, 2,5-dimethoxyphenyl ring), 7.65 (d, 2H, J = 7.8 Hz, *p*-methoxyphenyl ring), 7.85 (d, 1H, J = 8.3 Hz, 2,5-dimethoxyphenyl ring), 8.68 (s, *br*, 2H, NH_2 exchangeable by D_2O), 9.34, 10.06 (2s, 2H, 2NH exchangeable by D_2O); Anal. Calcd. (%) for $C_{29}H_{25}N_7O_4$ (535.55): C, 65.04; H, 4.71; N, 18.31. Found: C, 65.24; H, 4.45; N, 18.65%.

7-Amino-*N*-(4-chlorophenyl)-6-cyano-2-(4-methoxyphenylamino)-5-(4-methylphenyl) pyrazolo[1,5-*a*]pyrimidine-3-carboxamide (14f)

Yellow crystals; M.p.: > 300 °C; Yield (76%); IR (KBr) ν_{max}/cm^{-1} 3439, 3296, 3234 (NH_2, 2NH), 2214 (C≡N), 1639 (C=O), 1595 (C=N), 1564 (C=C); ^{1}H NMR (500 MHz, DMSO-d_6, δ/ppm): 2.38 (s, 3H, CH_3), 3.70 (s, 3H, OCH_3), 6.85 (d, 2H, $J = 7.3$ Hz, *p*-methoxyphenyl ring), 7.36 (d, 4H, $J = 7.5$ Hz, ArH), 7.55 (d, 2H, $J = 6.2$ Hz, ArH), 7.74 (d, 2H, $J = 7.1$ Hz, ArH), 7.83 (d, 2H, $J = 7.7$ Hz, *p*-methoxyphenyl ring), 8.76 (s, *br*, 2H, NH_2), 9.06, 10.15 (2s, 2H, NH); MS (*m/z*, %): 525 (M^{+2}, 25.41), 523 (M^+, 76.85), 93 (base peak, 100%); Anal. Calcd. (%) for $C_{28}H_{22}ClN_7O_2$ (523.97): C, 64.18; H, 4.23; N, 18.71. Found: C, 64.35; H, 4.05; N, 18.48.

7-Amino-*N*-(4-chlorophenyl)-6-cyano-2-(4-methoxyphenylamino)-5-(3-methylphenyl) pyrazolo[1,5-*a*]pyrimidine-3-carboxamide (14g)

Yellow crystals; M.p.: > 300 °C; Yield (71%); IR (KBr) ν_{max}/cm^{-1} 3419, 3335 (NH_2, 2NH), 2216 (C≡N), 1651 (C=O), 1592 (C=N), 1554 (C=C); ^{1}H NMR (500 MHz, DMSO-d_6, δ/ppm): 2.44 (s, 3H, CH_3), 3.74 (s, 3H, OCH_3), 6.89 (d, 2H, $J = 8.9$ Hz, *p*-methoxyphenyl ring), 7.40 (d, 2H, $J = 8.9$ Hz, *p*-chlorophenyl ring), 7.44 (d, 1H, $J = 7.7$ Hz, *m*-methylphenyl ring), 7.49 (t, 1H, $J = 7.6$ Hz, *m*-methylphenyl ring), 7.58 (d, 2H, $J = 8.8$ Hz, *p*-chlorophenyl ring), 7.77 (d, 1H, $J = 7.7$ Hz, *m*-methylphenyl ring), 7.80 (s, 1H, *m*-methylphenyl ring), 7.82 (d, 2H, $J = 8.9$ Hz, *p*-methoxyphenyl ring), 9.00 (s, *br*, 2H, NH_2 exchangeable by D_2O), 9.12, 10.21 (2s, 2H, 2NH exchangeable by D_2O); Anal. Calcd. (%) for $C_{28}H_{22}ClN_7O_2$ (523.97): C, 64.18; H, 4.23; N, 18.71. Found: C, 64.02; H, 4.54; N, 18.52%.

7-Amino-*N*-(4-chlorophenyl)-6-cyano-5-(3-methoxyphenyl)-2-(4-methoxyphenylamino) pyrazolo[1,5-*a*]pyrimidine-3-carboxamide (14h)

Yellow crystals; M.p.: > 300 °C; Yield (73%); IR (KBr) ν_{max}/cm^{-1} 3436, 3307 (NH_2, 2NH), 2213 (C≡N), 1643 (C=O), 1603 (C=N), 1544 (C=C); ^{1}H NMR (500 MHz, DMSO-d_6, δ/ppm): 3.74, 3.86 (2s, 6H, $2OCH_3$), 6.90 (d, 2H, $J = 9.1$ Hz, *p*-methoxyphenyl ring), 7.18–7.20 (m, 1H, *m*-methoxyphenyl ring), 7.42 (d, 2H, $J = 8.8$ Hz, *p*-chlorophenyl ring), 7.51–7.55 (m, 3H, $J = 7.7$ Hz, *m*-methoxyphenyl ring), 7.62 (d, 2H, $J = 8.9$ Hz, *p*-chlorophenyl ring), 7.84 (d, 2H, $J = 9.0$ Hz, *p*-methoxyphenyl ring), 8.99 (s, *br*, 2H, NH_2 exchangeable by D_2O), 9.17, 10.18 (2s, 2H, 2NH exchangeable by D_2O); Anal. Calcd. (%) for $C_{28}H_{22}ClN_7O_3$ (539.97): C, 62.28; H, 4.11; N, 18.16. Found: C, 62.35; H, 4.05; N, 18.34%.

7-Amino-5-(3-chlorophenyl)-*N*-(4-chlorophenyl)-6-cyano-2-(4-methoxyphenylamino)pyrazolo[1,5-*a*]pyrimidine-3-carboxamide (14i) [61]

Yellow crystals; M.p. 252–254 ºC; Yield (71%); IR (KBr) ν_{max}/cm^{-1} 3397, 3308 (NH_2, 2NH), 2211 (C≡N), 1652 (C=O), 1613 (C=N), 1547 (C=C); ^{1}H NMR (400 MHz, DMSO-d_6, $CDCl_3$, δ/ppm): 3.73 (s, 3H, OCH_3), 6.82 (d, 2H, $J = 8.8$ Hz, ArH), 7.16–7.22 (m, 2H, ArH), 7.52 (d, 2H, $J = 7.8$ Hz, ArH), 7.60 (d, 2H, $J = 8.8$ Hz, ArH), 7.66 (d, 1H, $J = 8.8$ Hz, ArH), 7.81–7.91 (m, 3H, ArH), 8.63 (s, *br*, 2H, NH_2 exchangeable by D_2O), 9.14, 10.02 (2s, 2H, 2NH exchangeable by D_2O); ^{13}C NMR (100 MHz, DMSO-d_6, $CDCl_3$, δ/ppm): 55.52 (1C, OCH_3), 75.48, 89.92, 114.36, 115.87, 119.28, 120.51, 127.13, 127.89, 128.34, 129.01, 130.38, 131.00, 133.49, 134.24, 134.93, 137.49, 145.89, 149.54, 154.42, 156.98, 161.21, 163.20 (26C); Anal. Calcd. (%) for $C_{27}H_{19}Cl_2N_7O_2$ (544.39): C, 59.57; H, 3.52; N, 18.01. Found: C, 59.49; H, 3.60; N, 17.95%.

7-Amino-*N*-(4-chlorophenyl)-6-cyano-5-(2,5-dimethoxyphenyl)-2-(4-methoxyphenylamino) pyrazolo[1,5-*a*]pyrimidine-3-carboxamide (14j)

Yellow crystals; M.p.: > 300 °C; Yield (74%); IR (KBr) ν_{max}/cm^{-1} 3446, 3310 (NH_2, 2NH), 2215 (C≡N), 1637 (C=O), 1596 (C=N), 1568 (C=C); ^{1}H NMR (500 MHz, DMSO-d_6, δ/ppm): 3.70, 3.75, 3.78 (3s, 9H, $3OCH_3$), 6.86 (d, 2H, $J = 9.5$ Hz, *p*-methoxyphenyl ring), 7.10–7.17 (m, 3H, 2,5-dimethoxyphenyl ring), 7.34 (d, 2H, $J = 9.2$ Hz, *p*-chlorophenyl ring), 7.48 (d, 2H, $J = 9.2$ Hz, *p*-chlorophenyl ring), 7.78 (d, 2H, $J = 9.3$ Hz, *p*-methoxyphenyl ring), 8.97 (s, *br*, 2H, NH_2 exchangeable by D_2O), 9.11, 10.04 (2s, 2H, 2NH exchangeable by D_2O); ^{13}C NMR (125 MHz, DMSO-d_6, δ/ppm): 55.12, 55.68, 55.93 (3C, $3OCH_3$), 78.02, 88.84, 104.95, 113.21, 114.13, 115.17, 117.23, 118.96, 120.38, 126.91, 128.90, 133.25, 137.20, 145.72, 148.51, 150.65, 153.07, 153.91, 156.07, 159.97, 159.99, 162.09 (26C); Anal. Calcd. (%) for $C_{29}H_{24}ClN_7O_4$ (570.00): C, 61.11; H, 4.24; N, 17.20. Found: C, 60.90; H, 4.39; N, 17.48%.

Synthesis of Schiff bases 16a-j

A mixture of 5-amino-*N*-aryl-1*H*-pyrazole-4-carboxamide derivatives **9a**, **b** (0.01 mol) and various aldehydes **15a–e** (0.01 mol) {namely: 3-methoxybenzaldehyde (**15a**), 4-(dimethylamino)benzaldehyde (**15b**), 2,5-dimethoxybenzaldehyde (**15c**), 4-chloro-3-nitrobenzaldehyde (**15d**), or thiophene-2-carbaldehyde **(15e)**} with a catalytic amount of glacial acetic acid (1 mL) in absolute ethanol (25 mL) was

refluxed for 2 h and then left to cool. The solid product was filtered off, dried and finally recrystallized from ethanol to afford the corresponding Schiff bases **16a–j**.

5-(3-Methoxybenzylideneamino)-3-(4-methoxyphenylamino)-*N*-phenyl-1*H*-pyrazole-4-carboxamide (16a)

Yellow crystals; M.p.: 201–203 °C; Yield (75%); IR (KBr) ν_{max}/cm^{-1} 3434, 3229 (3NH), 1656 (C=O), 1612 (C=N), 1587 (C=C); ^{1}H NMR (500 MHz, DMSO-d_6, δ/ppm): 3.73, 3.88 (2s, 6H, $2OCH_3$), 6.91 (d, 2H, $J=8.3$ Hz, *p*-methoxyphenyl ring), 7.08 (t, 1H, $J=7.4$ Hz, phenyl ring), 7.23 (d, 1H, $J=7.5$ Hz, *m*-methoxyphenyl ring), 7.36 (t, 2H, $J=7.9$ Hz, phenyl ring), 7.55 (t, 1H, $J=7.8$ Hz, *m*-methoxyphenyl ring), 7.62–7.64 (m, 4H, phenyl ring + *m*-methoxyphenyl ring), 7.68 (d, 2H, $J=8.0$ Hz, *p*-methoxyphenyl ring), 8.71 (s, 1H, –CH=N–), 9.05, 9.99, 12.80 (3s, 3H, 3NH exchangeable by D_2O); ^{13}C NMR (125 MHz, DMSO-d_6, δ/ppm): 55.27, 55.34 (2C, $2OCH_3$), 83.17, 112.33, 114.51, 118.98, 119.82, 123.30, 128.54, 129.08, 129.37, 130.53, 135.02, 138.54, 146.21, 152.25, 155.38, 156.89, 159.83, 161.70, 162.69 (23C); MS (*m/z*, %): 441 (M^+, 25.67%), 83 (base peak, 100%); Anal. Calcd. (%) for $C_{25}H_{23}N_5O_3$ (441.48): C, 68.01; H, 5.25; N, 15.86. Found: C, 68.17; H, 5.06; N, 15.69%.

5-(4-(Dimethylamino)benzylideneamino)-3-(4-methoxyphenylamino)-*N*-phenyl-1*H*-pyrazole-4-carboxamide (16b) [62]

Yellow crystals; M.p.: 216–218 °C; Yield (87%); IR (KBr) ν_{max}/cm^{-1} 3445, 3292 (3NH), 1652 (C=O), 1614 (C=N), 1592 (C=C); ^{1}H NMR (400 MHz, DMSO-d_6, δ/ppm): 3.01 (s, 6H, $N(CH_3)_2$), 3.66 (s, 3H, OCH_3), 6.83 (d, 4H, $J=8.9$ Hz, ArH), 7.02 (t, 1H, ArH), 7.33 (t, 2H, ArH), 7.48 (2H, ArH), 7.60 (d, 2H, $J=8.4$ Hz, ArH), 7.80 (d, 2H, $J=8.7$ Hz, ArH), 8.67 (s, 1H, –N=CH–), 9.03, 10.07, 12.59 (3s, 3H, 3NH exchangeable by D_2O); ^{13}C NMR (100 MHz, DMSO-d_6, δ/ppm) δ 40.10 (2C, N $(CH_3)_2$ under solvent DMSO), 55.48 (OCH_3), 92.74, 112.34, 115.12, 120.08, 121.82, 126.58, 128.07, 128.43, 129.19, 132.02, 132.84, 135.21, 152.78, 153.40, 153.84, 154.45, 160.57, 162.06 (23C); Anal. Calcd. (%) for $C_{26}H_{26}N_6O_2$ (454.52): C, 68.70; H, 5.77; N, 18.49. Found: C, 68.75; H, 5.70; N, 18.55%.

5-(2,5-Dimethoxybenzylideneamino)-3-(4-methoxyphenylamino)-*N*-phenyl-1*H*-pyrazole-4-carboxamide (16c)

Orange crystals; M.p.: 234–236 °C; Yield (69%); IR (KBr) ν_{max}/cm^{-1} 3389, 3320 (3NH), 1654 (C=O), 1594 (C=N), 1552 (C=C); ^{1}H NMR (500 MHz, DMSO-d_6, δ/ppm): 3.72, 3.83, 3.89 (3s, 9H, $3OCH_3$), 6.91 (d, 2H, $J=8.0$ Hz, *p*-methoxyphenyl ring), 7.08–7.35 (m, 7H, Ar–H), 7.50 (s, 1H, 2,5-dimethoxyphenyl ring), 7.65 (d, 2H, $J=8.3$ Hz, *p*-methoxyphenyl ring), 8.69 (s, 1H, –CH=N–), 9.47, 10.18, 13.01 (3s, 3H, 3NH exchangeable by D_2O); Anal. Calcd. (%) for $C_{26}H_{25}N_5O_4$ (471.51): C, 66.23; H, 5.34; N, 14.85. Found: C, 66.62; H, 5.17; N, 14.68%.

5-(4-Chloro-3-nitrobenzylideneamino)-3-(4-methoxyphenylamino)-*N*-phenyl-1*H*-pyrazole-4-carboxamide (16d)

Buff crystals; M.p.: 252–254 °C; Yield (72%); IR (KBr) ν_{max}/cm^{-1} 3431, 3235 (3NH), 1653 (C=O), 1615 (C=N), 1513 (C=C); ^{1}H NMR (500 MHz, DMSO-d_6, δ/ppm): 3.70 (s, 3H, OCH_3), 6.89 (d, 2H, $J=8.3$ Hz, *p*-methoxyphenyl ring), 7.06 (t, 1H, $J=7.3$ Hz, phenyl ring), 7.31–7.34 (m, 4H, phenyl ring), 7.67 (d, 2H, $J=7.9$ Hz, *p*-methoxyphenyl ring), 8.00 (d, 1H, $J=8.3$, 4-chloro-3-nitrophenyl ring), 8.30 (d, 1H, $J=8.3$, 4-chloro-3-nitrophenyl ring), 8.67 (s, 1H, 4-chloro-3-nitrophenyl ring), 8.76 (s, 1H, –CH=N–), 9.13, 9.79, 12.80 (3s, 3H, 3NH exchangeable by D_2O); ^{13}C NMR (125 MHz, DMSO-d_6, δ/ppm): 55.23 (1C, OCH_3), 96.78, 114.61, 118.92, 119.73, 121.51, 123.06, 125.26, 126.27, 128.87, 132.72, 133.81, 134.09, 138.39, 147.84, 152.02, 153.37, 157.62, 160.86, 162.42 (23C); Anal. Calcd. (%) for $C_{24}H_{19}ClN_6O_4$ (490.90): C, 58.72; H, 3.90; N, 17.12; Found: C, 58.99; H, 3.79; N, 17.28%.

3-(4-Methoxyphenylamino)-*N*-phenyl-5-(thiophen-2-ylmethyleneamino)-1*H*-pyrazole-4-carboxamide (16e)

Yellow crystals; M.p.: 212–214 °C; Yield (67%); IR (KBr) ν_{max}/cm^{-1} 3433, 3272 (3NH), 1652 (C=O), 1594 (C=N), 1547 (C=C); ^{1}H NMR (500 MHz, DMSO-d_6, δ/ppm): 3.73 (s, 3H, OCH_3), 6.90 (d, 2H, $J=7.1$ Hz, *p*-methoxyphenyl ring), 7.09 (d, 1H, $J=5.3$ Hz, thiophene ring), 7.33–7.40 (m, 5H, phenyl ring), 7.72 (d, 2H, $J=7.0$ Hz, *p*-methoxyphenyl ring), 7.91 (d, 1H, $J=3.6$ Hz, thiophene ring), 8.05 (s, 1H, thiophene ring), 8.68 (s, 1H, –CH=N–), 9.19, 9.98, 12.50 (3s, 3H, 3NH exchangeable by D_2O); ^{13}C NMR (125 MHz, DMSO-d_6, δ/ppm): 55.79 (1C, OCH_3), 89.70, 115.01, 119.23, 123.68, 129.62, 129.74, 133.89, 134.14, 134.29, 136.99, 139.23, 141.83, 155.79, 156.45, 157.46, 159.54, 163.28 (21C); MS (*m/z*, %): 417 (M^+, 18.85%), 186 (base peak, 100%); Anal. Calcd. (%) for $C_{22}H_{19}N_5O_2S$ (417.48): C, 63.29; H, 4.59; N, 16.78; Found: C, 63.45; H, 4.39; N, 16.85%.

N-(4-Chlorophenyl)-5-(3-methoxybenzylideneamino)-3-(4-methoxyphenylamino)-1*H*-pyrazole-4-carboxamide (16f)

Yellow crystals; M.p.: 205–207 °C; Yield (73%); IR (KBr) ν_{max}/cm^{-1} 3434, 3229 (3NH), 1656 (C=O), 1612 (C=N), 1587 (C=C); ^{1}H NMR (500 MHz, DMSO-d_6, δ/ppm): 3.73, 3.87 (2s, 6H, $2OCH_3$), 6.90 (d, 2H, $J=8.9$ Hz, *p*-methoxyphenyl ring), 7.21, 7.23 (dd, 1H, $J=8.2$, 1.8 Hz,

m-methoxyphenyl ring), 7.40 (d, 4H, $J = 8.9$ Hz, *p*-chlorophenyl ring), 7.53 (t, 1H, $J = 7.9$ Hz, *m*-methoxyphenyl ring), 7.59 (s, 1H, *m*-methoxyphenyl ring), 7.62 (d, 1H, $J = 2.4$ Hz, *m*-methoxyphenyl ring), 7.69 (d, 2H, $J = 8.9$ Hz, *p*-methoxyphenyl ring), 8.66 (s, 1H, –CH=N–), 9.03, 10.02, 12.78 (3s, 3H, 3NH exchangeable by D_2O); ^{13}C NMR (125 MHz, DMSO-d_6, δ/ppm): 55.19, 55.23 (2C, $2OCH_3$), 92.61, 112.24, 114.39, 119.22, 119.53, 120.41, 122.48, 126.69, 128.34, 128.73, 130.28, 133.79, 136.17, 137.46, 151.21, 154.04, 159.74, 162.03, 162.65 (23C); Anal. Calcd. (%) for $C_{25}H_{22}ClN_5O_3$ (475.93): C, 63.09; H, 4.66; N, 14.72; Found: C, 63.34; H, 4.53; N, 14.43%.

N-(4-Chlorophenyl)-5-(4-(dimethylamino)benzylideneamino)-3-(4-methoxyphenylamino)-1*H*-pyrazole-4-carboxamide (16g) [62]

Yellow crystals; M.p.: 209–211 °C, Yield (86%); IR (KBr) ν_{max}/cm^{-1} 3431, 3275 (3NH), 1662 (C=O), 1609 (C=N), 1581 (C=C); ^1H NMR (400 MHz, DMSO-d_6, δ ppm): 3.38 (s, 6H, $N(CH_3)_2$), 3.71 (s, 3H, OCH_3), 6.85 (d, 2H, $J = 9$ Hz, *p*-dimethylaminophenyl ring), 6.88 (d, 2H, $J = 8.9$ Hz, *p*-methoxyphenyl ring), 7.40 (d, 2H, $J = 8.6$ Hz, *p*-chlorophenyl ring), 7.45 (d, 2H, $J = 8.5$ Hz, *p*-chlorophenyl ring), 7.68 (d, 2H, $J = 8.6$ Hz, *p*-methoxyphenyl ring), 7.82 (d, 2H, $J = 8.5$ Hz, *p*-dimethylaminophenyl ring), 8.66 (s, 1H, –CH=N–), 8.74, 10.24, 12.24 (3s, 3H, 3NH exchangeable by D_2O); ^{13}C NMR (100 MHz, DMSO-d_6, δ ppm): 40.06 (2C, N $(CH_3)_2$ under solvent DMSO), 55.67 (1C, OCH_3), 92.48, 112.27, 114.78, 120.87, 121.08, 122.12, 127.29, 129.43, 132.02, 133.35, 135.00, 152.88, 153.70, 153.89, 154.25, 161.19, 163.66 (23C); Anal. Calcd. (%) for $C_{26}H_{25}ClN_6O_2$ (488.97): C, 63.86; H, 5.15; N, 17.19; Found: C, 63.95; H, 5.10; N, 17.25%.

N-(4-Chlorophenyl)-5-(2,5-dimethoxybenzylideneamino)-3-(4-methoxyphenylamino)-1*H*-pyrazole-4-carboxamide (16h)

Orange crystals; M.p.: 250–252 °C; Yield (74%); IR (KBr) ν_{max}/cm^{-1} 3432, 3251 (3NH), 1653 (C=O), 1597 (C=N), 1544 (C=C); ^1H NMR (500 MHz, DMSO-d_6, δ/ppm): 3.73, 3.82, 3.88 (3s, 9H, $3OCH_3$), 6.89, 6.91 (dd, 2H, $J = 2.8$ & 9.5 Hz, *p*-methoxyphenyl ring), 7.18 (d, 1H, $J = 2.8$ Hz, 2,5-dimethoxyphenyl ring), 7.21 (d, 1H, $J = 2.7$ Hz, 2,5-dimethoxyphenyl ring), 7.38 (d, 2H, $J = 9.2$ Hz, *p*-chlorophenyl ring), 7.42 (d, 2H, $J = 9.0$ Hz, *p*-chlorophenyl ring), 7.61 (s, 1H, 2,5-dimethoxyphenyl ring), 7.66, 7.68 (dd, 2H, $J = 9.2$, 2.7 Hz, *p*-methoxyphenyl ring), 8.64 (s, 1H, –CH=N–), 9.34, 10.13, 11.74 (3s, 3H, 3NH exchangeable by D_2O); ^{13}C NMR (125 MHz, DMSO-d_6, δ/ppm): 55.26, 55.59, 56.47 (3C, $3OCH_3$), 92.55, 109.44, 114.21, 114.42, 119.00, 120.58, 121.94, 123.30, 126.66, 128.83, 134.18, 137.62, 153.41, 153.81, 154.87, 156.70, 156.90, 160.72, 162.88 (23C); Anal. Calcd. (%) for $C_{26}H_{24}ClN_5O_4$ (505.95): C, 61.72; H, 4.78; N, 13.84; Found: C, 61.90; H, 4.51; N, 13.98%.

5-(4-Chloro-3-nitrobenzylideneamino)-*N*-(4-chlorophenyl)-3-(4-methoxyphenylamino)-1*H*-pyrazole-4-carboxamide (16i)

Yellow crystals; M.p.: 280–282 °C; yield (71%); IR (KBr) ν_{max}/cm^{-1} 3440, 3280, 3230 (3NH), 1653 (C=O), 1615 (C=N), 1561 (C=C); ^1H NMR (500 MHz, DMSO-d_6, δ/ppm): 3.72 (s, 3H, OCH_3), 6.89 (d, 2H, $J = 8.7$ Hz, *p*-methoxyphenyl ring), 7.35 (d, 4H, $J = 8.8$ Hz, *p*-chlorophenyl ring), 7.70 (d, 2H, $J = 8.8$ Hz, *p*-methoxyphenyl ring), 7.96 (d, 1H, $J = 8.4$ Hz, 4-chloro-3-nitrophenyl ring), 8.27 (d, 1H, $J = 8.3$ Hz, 4-chloro-3-nitrophenyl ring), 8.26 (s, 1H, 4-chloro-3-nitrophenyl ring), 8.72 (s, 1H, –CH=N–), 9.14, 9.87, 12.94 (3s, 3H, 3NH exchangeable by D_2O); Anal. Calcd. (%) for $C_{24}H_{18}Cl_2N_6O_4$ (525.34): C, 54.87; H, 3.45; N, 16.00; Found: C, 55.05; H, 3.28; N, 16.19%.

N-(4-Chlorophenyl)-3-(4-methoxyphenylamino)-5-(thiophen-2-ylmethyleneamino)-1*H*-pyrazole-4-carboxamide (16j)

Yellow crystals; M.p.: 221–223 °C; yield (68%); IR (KBr) ν_{max}/cm^{-1} 3432, 3278 (3NH), 1653 (C=O), 1598 (C=N), 1562 (C=C); ^1H NMR (500 MHz, DMSO-d_6, δ/ppm): 3.73 (s, 3H, OCH_3), 6.91 (d, 2H, $J = 8.1$ Hz, *p*-methoxyphenyl ring), 7.39–7.45 (m, 5H, *p*-chlorophenyl ring + thiophene ring), 7.74 (d, 2H, $J = 8.0$ Hz, *p*-methoxyphenyl ring), 7.91 (d, 1H, $J = 2.3$ Hz, thiophene ring), 8.05 (d, 1H, $J = 4.8$ Hz, thiophene ring), 8.64 (s, 1H, –CH=N–), 9.19, 10.04, 12.97 (3s, 3H, 3NH exchangeable by D_2O); Anal. Calcd. (%) for $C_{22}H_{18}ClN_5O_2S$ (451.93): C, 58.47; H, 4.01; N, 15.50; Found: C, 58.58; H, 4.19; N, 15.21%.

In vitro antimicrobial evaluation

Microorganisms

The microbes used in this study were Gram-positive bacterial strain (*Bacillus subtilis* ATCC-6633), Gram-negative bacterial strain (*Escherichia coli* ATCC-25922), yeast (*Candida albicans* ATCC-10231), and *Aspergillus niger* NRRL-3 as fungi. These microorganisms were obtained from the American Type Culture Collection (ATCC, Rockville, MD, USA) and Northern Utilization Research and Development Division, United State Department of Agriculture, Peoria, Illinois, USA (NRRL). The bacterial strains were revived for bonsai by sub-culturing fresh nutrient agar (NA) medium (Merck, Darmstadt, Germany) for 24 h before the test, while, fungi were cultured on potato dextrose agar (PDA) (Lab M.,

Bury, Lancashire, UK) for 7 days at 28 °C before the experiment was carried out.

Inoculum preparation

Stock cultures were maintained at 4 °C on slopes of nutrient agar and potato dextrose agar. Active cultures for experiments were prepared by transferring a lapful of cells from the stock cultures to test tubes of Mueller–Hinton broth (MHB) (Lab M Limited, Bury, Lancashire, UK) for bacteria and Sabouraud dextrose broth (SDB) (Lab M., Bury, Lancashire, UK) for fungi that were incubated without agitation for 24 h at 37 °C and 25 °C, respectively. To 5 mL of MHB and SDB, 0.2 mL of culture was inoculated and incubated (or diluted) till it reached the turbidity equal to that of the standard 0.5 McFarland solution at 625 nm ($A = 0.08$ to 0.1) which is equivalent to 1.5×10^8 cfu.mL^{-1}.

Bioassay method

Agar diffusion technique as described by Perez et al. [45] was used to determine the in vitro antibacterial activity of the powder samples. A 0.1 mL aliquot of 18 h broth culture of the above-mentioned bacteria that had been adjusted to the turbidity equivalent of 0.5 McFarland standards [63] was dispensed into sterile Petri dishes previously labeled with the test bacteria. Molten sterile Muller-Hinton was aseptically poured into the plates and gently rotated for the bacteria to be homogeneously distributed in the medium. The agar plates were allowed to solidify. The antibacterial screening bioassay was made by the agar well diffusion method described by Jorgensen and Turnidge [64] using Mueller–Hinton agar (Lab M Limited, Bury, Lancashire, UK), then the plates allowed to diffuse for two hours at 4 °C. The experiment was conducted in triplicates. All plates were incubated at 37 °C for 24 h for bacterial strains and 28–30 °C for 48 h for fungal strain. Clearance zones around the wells were noted and measured in millimeters [65]. Standard bacterial antibiotics as Tetracycline (30 µg) and Novobiocine (30 µg) and fungal antibiotic as Clotrimazole (50 µg), and Cyclohexamide (50 µg) were used as a positive control for bacteria and fungi, respectively.

Molecular docking

All the molecular docking studies were performed using Molecular Operating Environmental (MOE) software 2008.10. The most active derivatives against the tested bacterial strains (**14b**, **14e**, **14j**, and **16i**) and fungal pathogens (**16c**, **16d**, **16h**, and **16i**) were builders using ChemDraw 2014. The structure of the most active derivatives was protonated and minimized energy using MMFF94X force field with a root mean standard deviation (RMSD) gradient of 0.05 kcal mol^{-1} Å as well as the partial charged calculated. For promising antibacterial derivatives *S. aureus* Gyrase complex with Ciprofloxacin (PDB:2XCT), and for promising fungal derivatives secreted aspartic protease from *C. albicans* (PDB: 1ZAP) were selected for this study [57, 58]. The enzyme with its co-crystallized ligand was retrieved from the protein data bank. For DNA gyrase (PDB:2XCT), the docking process performed using only one chain G chain only according to the reported method. For fungal, the protein structure (PDB: 1ZAP) contains only one chain (A). The enzyme was prepared according to default protocol by removing the water molecules, hydrogen atom added. The alpha site finder was used to generate the active site. For docking studies, the trigonal matcher placement and the London dG scoring function were selected after redocking the co-crystalized ligand in both enzymes.

Supplementary Information The online version contains supplementary material available at https://doi.org/10.1007/s13738-021-02319-4.

Acknowledgements The authors wish to express their thanks to the National Research Centre for the facilities provided.

Declarations

Conflict of interest The authors declare that they have no conflict of interest.

References

1. M.A. Hosny, Y.H. Zaki, W.A. Mokbel, A.O. Abdelhamid, Med Chem. **16**, 750–760 (2020). https://doi.org/10.2174/1573406415666190620144404
2. S. Oh, M.D.J. Libardo, S. Azeeza, G.T. Pauly, J.S.O. Roma, A. Sajid, Y. Tateishi, C. Duncombe, M. Goodwin, T.R. Ioerger, P.G. Wyatt, P.C. Ray, D.W. Gray, H.I.M. Boshoff, C.E. Barry, ACS Infect Dis. **7**, 479–492 (2021). https://doi.org/10.1021/acsinfecdis.0c00851
3. M.A. Salem, M.H. Helal, M.A. Gouda, H.H. Abd EL-Gawad, M.A.M. Shehab, A. El-Khalafawy, Synth. Commun. **49**, 1750–1776 (2019). https://doi.org/10.1080/00397911.2019.1604967
4. A.M. Fahim, A.M. Farag, J. Mol. Struct. **1199**, 127025 (2020). https://doi.org/10.1016/j.molstruc.2019.127025
5. S. Cherukupalli, R. Karpoormath, B. Chandrasekaran, G.A. Hampannavar, N. Thapliyal, V.N. Palakollu, Eur. J. Med. Chem. **126**, 298–352 (2017). https://doi.org/10.1016/j.ejmech.2016.11.019
6. Y.V. Burgart, N.A. Elkina, E.V. Shchegolkov, O.P. Krasnykh, V.V. Maslova, G.A. Triandafilova, S.Y. Solodnikov, G.F. Makhaeva, O.G. Serebryakova, E.V. Rudakova, V.I. Saloutin, Chem. Heterocycl. Compds. **56**, 199–207 (2020). https://doi.org/10.1007/s10593-020-02652-1
7. M.H. Attia, E.Z. Elrazaz, S.Z. El-Emam, A.T. Taher, H.A. Abdel-Aziz, K.A.M. Abouzid, Bioorg. Chem. **94**, 103458 (2020). https://doi.org/10.1016/j.bioorg.2019.103458
8. L.-L. He, Q. Qi, X. Wang, Y. Li, Y. Zhu, X.-F. Wang, L. Xu, Bioorg. Chem. **99**, 103833 (2020). https://doi.org/10.1016/j.bioorg.2020.103833

9. A.M. Naglah, A.A. Askar, A.S. Hassan, T.K. Khatab, M.A. Al-Omar, M.A. Bhat, Molecules **25**, 1431 (2020). https://doi.org/10.3390/molecules25061431
10. M. El-Naggar, A.S. Hassan, H.M. Awad, M.F. Mady, Molecules **23**, 1249 (2018). https://doi.org/10.3390/molecules23061249
11. A.Y. Hassan, N.M. Saleh, M.S. Kadh, E.S. Abou-Amra, J. Heterocyclic Chem. **57**, 2704–2721 (2020). https://doi.org/10.1002/jhet.3979
12. A.M. Vijesh, A.M. Isloor, P. Shetty, S. Sundershan, H.K. Fun, Eur. J. Med. Chem. **62**, 410–415 (2013). https://doi.org/10.1016/j.ejmech.2012.12.057
13. N.M. Morsy, A.S. Hassan, T.S. Hafez, M.R.H. Mahran, I.A. Sadawe, A.M. Gbaj, J. Iran. Chem. Soc. **18**, 47–59 (2021). https://doi.org/10.1007/s13738-020-02004-y
14. A.S. Hassan, A.A. Askar, A.M. Naglah, A.A. Almehizia, A. Ragab, Molecules **25**, 2593 (2020). https://doi.org/10.3390/molecules25112593
15. S.Ö. Ozkınalı, M. Gür, N. Şener, S. Alkın, M.S. Çavuş, J. Mol. Struct. **1174**, 74–83 (2018). https://doi.org/10.1016/j.molstruc.2018.06.070
16. A.S. Hassan, T.S. Hafez, S.A. Osman, M.M. Ali, Turk. J. Chem. **39**, 1102–1113 (2015). https://doi.org/10.3906/kim-1504-12
17. K. Singh, Y. Kumar, P. Puri, M. Kumar, C. Sharma, Eur. J. Med. Chem. **52**, 313–321 (2012). https://doi.org/10.1016/j.ejmech.2012.02.053
18. A.S. Hassan, G.O. Moustafa, A.A. Askar, A.M. Naglah, M.A. Al-Omar, Synth. Commun. **48**, 2761–2772 (2018). https://doi.org/10.1080/00397911.2018.1524492
19. S. Malladi, A.M. Isloor, S. Isloor, D.S. Akhila, H.-K. Fun, Arabian J. Chem. **6**, 335–340 (2013). https://doi.org/10.1016/j.arabjc.2011.10.009
20. A.S. Hassan, G.O. Moustafa, N.M. Morsy, A.M. Abdou, T.S. Hafez, Egypt. J. Chem. **63**, 4469–4481 (2020). https://doi.org/10.21608/ejchem.2020.26158.2525
21. A.S. Hassan, A.A. Askar, E.S. Nossier, A.M. Naglah, G.O. Moustafa, M.A. Al-Omar, Molecules **24**, 3130 (2019). https://doi.org/10.3390/molecules24173130
22. A.S. Hassan, Bull. Chem. Soc. Ethiop. **34**, 533–541 (2020). https://doi.org/10.4314/bcse.v34i3.9
23. T.K. Khatab, A.S. Hassan, T.S. Hafez, Bull. Chem. Soc. Ethiop. **33**, 135–142 (2019). https://doi.org/10.4314/bcse.v33i1.13
24. A.A. Magd-El-Din, H.A. Mousa, A.A. Labib, A.S. Hassan, A.S. AbdEl-All, M.M. Ali, A.A. El-Rashedy, A.H. El-Desoky, Z. Naturforsch. C **73**, 465–478 (2018). https://doi.org/10.1515/znc-2018-0010
25. S.S. Mukhtar, A.S. Hassan, N.M. Morsy, T.S. Hafez, F.M. Saleh, H.M. Hassaneen, Synth. Commun. **51**, 1564–1580 (2021). https://doi.org/10.1080/00397911.2021.1894338
26. A.S. Hassan, T.S. Hafez, J. Appl. Pharm. Sci. **8**, 156–165 (2018). https://doi.org/10.7324/JAPS.2018.8522
27. A.S. Hassan, G.O. Moustafa, H.M. Awad, Synth. Commun. **47**, 1963–1972 (2017). https://doi.org/10.1080/00397911.2017.1358368
28. A.S. Hassan, T.S. Hafez, M.M. Ali, T.K. Khatab, Res. J. Pharm. Biol. Chem. Sci. **7**, 417–429 (2016)
29. A.S. Hassan, S.A. Osman, T.S. Hafez, Egypt. J. Chem. **58**, 113–139 (2015). https://doi.org/10.21608/ejchem.2015.978
30. A.S. Hassan, G.O. Moustafa, H.M. Awad, E.S. Nossier, M.F. Mady, ACS Omega **6**, 12361–12374 (2021). https://doi.org/10.1021/acsomega.1c01604
31. A.M. Abdelghany, T.K. Khatab, A.S. Hassan, Bull. Chem. Soc. Ethiop. **35**, 185–196 (2021). https://doi.org/10.4314/bcse.v35i1.16
32. T.S. Hafez, S.A. Osman, H.A.A. Yosef, A.S. Abd El-All, A.S. Hassan, A.A. El-Sawy, M.M. Abdallah, M. Youns, Sci. Pharm. **81**, 339–357 (2013). https://doi.org/10.3797/scipharm.1211-07
33. S.A. Osman, H.A.A. Yosef, T.S. Hafez, A.A. El-Sawy, H.A. Mousa, A.S. Hassan, Aust. J. Basic Appl. Sci. **6**, 852–863 (2012)
34. Y.A. Ammar, A.A. Farag, A.M. Ali, A. Ragab, A.A. Askar, D.M. Elsisi, A. Belal, Bioorg. Chem. **104**, 104164 (2020). https://doi.org/10.1016/j.bioorg.2020.104164
35. M.M.S. Wassel, W.M. Gamal Eldin, A. Ragab, G.A.M. Elhag Ali, Y.A. Ammar, J. Appl. Vet. Sci. **5**, 37–46 (2020). https://doi.org/10.21608/javs.2020.118001
36. M.M.S. Wassel, A. Ragab, G.A.M. Elhag Ali, A.B.M. Mehany, Y.A. Ammar, J. Mol. Struct. **1223**, 128966 (2021). https://doi.org/10.1016/j.molstruc.2020.128966
37. M.A. Salem, A. Ragab, A. El-Khalafawy, A.H. Makhlouf, A.A. Askar, Y.A. Ammar, Bioorg. Chem. **96**, 103619 (2020). https://doi.org/10.1016/j.bioorg.2020.103619
38. Y.A. Ammar, A.A. Farag, A.M. Ali, S.A. Hessein, A.A. Askar, E.A. Fayed, D.M. Elsisi, A. Ragab, Bioorg. Chem. **99**, 103841 (2020). https://doi.org/10.1016/j.bioorg.2020.103841
39. H.F. Rizk, M.A. El-Borai, A. Ragab, S.A. Ibrahim, J. Iran. Chem. Soc. **17**, 2493–2505 (2020). https://doi.org/10.1007/s13738-020-01944-9
40. Y.A. Ammar, S.Y. Abbas, M.A.M.S. El-Sharief, M.A.E.-R. Salem, A.R. Mohamed, Eur. J. Chem. **8**, 76–81 (2017). https://doi.org/10.5155/eurjchem.8.1.76-81.1542
41. A.S. Hassan, T.S. Hafez, S.A. Osman, Sci Pharm. **83**, 27–39 (2015). https://doi.org/10.3797/scipharm.1409-14
42. X.-S. Wang, Z.-S. Zeng, Y.-L. Li, D.-Q. Shi, S.-J. Tu, X.-Y. Wei, Z.-M. Zong, Synth. Commun. **35**, 1915–1920 (2005). https://doi.org/10.1081/SCC-200064966
43. A.M. Zonouz, D. Moghani, Synth. Commun. **41**, 2152–2160 (2011). https://doi.org/10.1080/00397911.2010.499488
44. A.S. Hassan, D.M. Masoud, F.M. Sroor, A.A. Askar, Med. Chem. Res. **26**, 2909–2919 (2017). https://doi.org/10.1007/s00044-017-1990-y
45. C. Perez, M. Paul, P. Bazerque, Acta. Bio. Med. Exp. **15**, 113–115 (1990)
46. M.A. El-sharief, S.Y. Abbas, M.A. Zahran, Y.A. Mohamed, A. Ragab, Y.A. Ammar, Z. Naturforsch. B **71**, 875–881 (2016). https://doi.org/10.1515/znb-2016-0054
47. A.K. Person, S.M. Chudgar, B.L. Norton, B.C. Tong, J.E. Stout, J. Med. Microbiol. **59**, 834–838 (2010). https://doi.org/10.1099/jmm.0.018309-0
48. E.A. Fayed, Y.A. Ammar, A. Ragab, N.A. Gohar, A.B.M. Mehany, A.M. Farrag, Bioorg. Chem. **100**, 103951 (2020). https://doi.org/10.1016/j.bioorg.2020.103951
49. A.S. Al Wasidi, A.S. Hassan, A.M. Naglah, J. Appl. Pharm. Sci. **10**, 142–148 (2020). https://doi.org/10.7324/JAPS.2020.104018
50. M.A. Elsherif, A.S. Hassan, G.O. Moustafa, H.M. Awad, N.M. Morsy, J. Appl. Pharm. Sci. **10**, 37–43 (2020). https://doi.org/10.7324/JAPS.2020.102006
51. E.M. Gad, M.S. Nafie, E.H. Eltamany, M.S.A.G. Hammad, A. Barakat, A.T.A. Boraei, Molecules **25**, 2523 (2020). https://doi.org/10.3390/molecules25112523
52. S. Ghannay, S. Bakari, M. Msaddek, S. Vidal, A. Kadri, K. Aouadi, Arabian J. Chem. **13**, 2121–2131 (2020). https://doi.org/10.1016/j.arabjc.2018.03.013
53. S. Ghannay, A. Kadri, K. Aouadi, Monatsh. Chem. **151**, 267–280 (2020). https://doi.org/10.1007/s00706-020-02550-4
54. X.Y. Meng, H.X. Zhang, M. Mezei, M. Cui, Curr. Comput Aided Drug Des. **7**, 146–157 (2011). https://doi.org/10.2174/157340911795677602
55. G. Wang, W. Zhu, Future Sci. (2016). https://doi.org/10.4155/fmc-2016-0143
56. K. Roy, S. Kar, R.N. Das, in *Understanding the Basics of QSAR for Applications in Pharmaceutical Sciences and Risk Assessment*. ed. by K. Roy, S. Kar, R.N. Das (Academic Press, Cambridge,

2015), pp. 357–425. https://doi.org/10.1016/B978-0-12-801505-6.00010-7
57. A. Ragab, S.A. Fouad, O.A.A. Ali, E.M. Ahmed, A.M. Ali, A.A. Askar, Y.A. Ammar, Antibiotics **10**, 162 (2021). https://doi.org/10.3390/antibiotics10020162
58. https://www.rcsb.org/structure/2XCT, and https://www.rcsb.org/structure/1ZAP. Accessed 21 Feb 2021
59. L.S.S. Andre, A.B.-S. Lys, Mini-Rev. Med. Chem. **13**, 155–162 (2013). https://doi.org/10.2174/138955713804484802
60. H.H. Khalil, S.N. Khattab, M.M. Toughan, A.M. El-Saghier, M.H. El-Wakil, ChemistrySelect **5**, 6556–6564 (2020). https://doi.org/10.1002/slct.202000886
61. A.S. Hassan, M.F. Mady, H.M. Awad, T.S. Hafez, Chin. Chem. Lett. **28**, 388–393 (2017). https://doi.org/10.1016/j.cclet.2016.10.022
62. A.S. Hassan, H.M. Awad, A.A. Magd-El-Din, T.S. Hafez, Med. Chem. Res. **27**, 915–927 (2018). https://doi.org/10.1007/s00044-017-2113-5
63. L.L. Zamora, M.T. Perez-Gracia, J. R. Soc. Interface **9**, 1892–1897 (2012). https://doi.org/10.1098/rsif.2011.0809
64. J.H. Jorgensen, J.D. Turnidge, in *Manual of Clinical Microbiology*. ed. by P.R. Murray, E.J. Baron, J.H. Jorgensen, M.L. Landry, M.A. Pfaller (ASM Press, Washington, 2007), pp. 1152–1172
65. M. Elgayyar, F.A. Draughon, D.A. Golden, J.R. Mount, J. Food Prot. **64**, 1019–1024 (2001). https://doi.org/10.4315/0362-028X-64.7.1019